

Abnormality Detection in Correlated Gaussian Molecular Nano-Networks: Design and Analysis

Siavash Ghavami and Farshad Lahouti

Abstract

A nano abnormality detection scheme (NADS) in molecular nano-networks is studied. This is motivated by the fact that early detection of diseases such as cancer play a crucial role in their successful treatment. The proposed NADS is in fact a two-tier network of sensor nano-machines (SNMs) in the first tier and a data-gathering node (DGN) at the sink. The SNMs detect the presence of competitor cells (abnormality) by variations in input and/or parameters of a nano-communications channel (NCC). The noise of SNMs as their nature suggest is considered correlated in time and space and herein assumed additive Gaussian. In the second step, the SNMs transmit micro-scale messages over a noisy micro communications channel (MCC) to the DGN, where a decision is made upon fusing the received signals. We find an optimum design of detectors for each of the NADS tiers based on the end-to-end NADS performance. The detection performance of each SNM is analyzed by setting up a generalized likelihood ratio test. Next, taking into account the effect of the MCC, the overall performance of the NADS is analyzed in terms of probabilities of misdetection and false alarm. In addition, computationally efficient expressions to quantify the NADS performance is derived by providing respectively an approximation and an upper bound for the probabilities of misdetection and false alarm. This in turn enables formulating a design problem, where the optimized concentration of SNMs in a sample is obtained for a high probability of detection and a limited probability of false alarm. The results indicate that otherwise ignoring the spatial and temporal correlation of SNM noise in the analysis, leads to an NADS that noticeably underperforms in operations.

Index Terms

Abnormality detection, Molecular communication, Mathematical modeling, Correlation.

S. Ghavami is with the Department of Electrical & Computer Engineering, University of Minnesota, USA and F. Lahouti is with the Electrical Engineering Department, California Institute of Technology, USA; E-mail: sghavami@umn.edu, lahouti@caltech.edu.

I. INTRODUCTION

Cancer is a leading cause of death in the world and accounts for about 13% of all death per annum [1]. In addition, it incurs serious disability and emotional challenges to the people and heavily affects them financially [2]. There have been many advances by significant technological innovations in the treatment of cancer. However, success is still a distant goal in this direction. Indeed, research in early detection and diagnostics of cancer and their associated enabling technologies are of extraordinary importance.

It is believed that the overall behavior of cancer is determined with genes expressions and/or proteins. In fact, proteomic data and collective functions of proteins are known to directly set the cell function. Hence, modeling and analysis of genomic and proteomic data using micro array and mass spectrometry technologies have found various applications in cancer studies [3]. In [4], an interesting review of technologies for nano-scale cancer bio-molecular detection using proteomic and genomic approaches is presented. In [5], application of nano-technologies for bio-molecular detection and medical diagnostics is studied. In [6] and [7], investigating the profile of molecules based on genetic expressions, reliable cancer classifiers are designed. The gene and/or protein changes due to certain types of cancer lead to peroxidation of cell membrane. This emits biomarkers in the blood or exhaled breath that may be detected using tailor-made cross-reactive sensors [8], [9]. A high level of insulin-like growth factor or estrogen in the blood of women before menopause is one sign of breast cancer [10]. In [11], combining engineered proteins with an appropriate detection technique is suggested to enable a new type of molecular sensor. Also in [12], nano-bio sensors are designed and simulated for dye molecules targeting to enhance targeting efficiency.

The development of novel mathematical models and analytical approaches for disease diagnostics in the nano-scale is crucial to take advantage of nano-technology for this purpose. The mathematical modeling and simulation of cancer progression are studied in [13] and [14], respectively. A model for nano-communications channel is proposed in [15], [16]. In [17], the noise in diffusion-based molecular communication over nano-networks is analyzed. The design of optimized molecular recognizers is studied in the biochemical noisy environment using a Bayesian cost in [18]. Such recognizers could serve as abnormality detection (AD) mechanisms by distinguishing between two molecule types, which one exists in the body on the healthy setting and the other appears only in the presence of a certain disease. In [19], a layered architecture of molecular communication is investigated. In practical schemes for

abnormality detection, one can typically identify a two-tier architecture for detection. In the first tier, the presence of abnormality is detected in the molecular nano-scale level. In the second tier, the abnormality is reported in a bigger scale to a data gathering node (DGN) in the outside world. A similar hierarchical architecture, which includes two levels of nano and micro scale messages is considered in [20] for body sensor networks. In [21], a two-tier nano abnormality detection scheme (NADS) in which the sensor nano-machines (SNMs) have independent Poisson observations [17] is suggested and its detection performance is analyzed.

Table I presents the two tiers of abnormality detection, i.e., detection in nano-scale and micro-scale, in different methods of cancer detection based on nano-technology. In detection of breast cancer, quantum dot bio-conjugates with targeting antibodies have been used to recognize associated molecular signatures including ERBB2 (Avian erythroblastosis oncogene B-2) [22], [23]. In the second tier, this feature is recognized using long-term multiple color imaging or immune-fluorescent labeling [22], [23]. In early detection of lung cancer, the increasing level of epidermal growth factor receptor (EGFR) can react at the nano-scale with injected single chain forward variable (SCFV) polypeptide with embedded Au [24], which act as a SNM. Next, the product of this reaction may be recognized by imaging techniques for finding Au in the body [25].

A potential candidate for SNM in NADS is graphene-based bio-sensors, which are optimized for detecting proteins, nucleic acids, carbohydrates, or compounds generated by metabolic processes. Existing detection methods employed by these sensors include electrical, electrochemical, and photonic approaches with respect to detecting labeled (or enzyme-assisted) and label-free (or enzyme-free) probe structures [45]. In this context, design and analysis of a wireless nanosensor network for monitoring human lung cells using graphene based sensors are considered in [46], where graphene antennas would be able to communicate in the terahertz band. In this case, respiration is the major process that influences the terahertz channel inside lung cells. The channel has been characterized as a two-state channel, where it periodically switches between good and bad states. It has been shown that the channel absorbs terahertz signal much faster when it is in the bad state as opposed to the good state [46]. Another reported application of in-vivo wireless network is graphene-based wireless bacteria detection on tooth enamel [47]. In this case, the DGN based on terminology of [48] is a so-called bio-cyber interface on the skin, which receives the electromagnetic signal transmitted by the graphene-based SNMs.

TABLE I: NADS in cancer detection using nano-technology.

Cancer detection method	Detection in tier 1-NCC	Detection in tier 2-MCC
Nano-sized magnetic resonance imaging (MRI) contrast agents for intraoperative imaging in the context of neuro-oncological interventions [26], [27]	Gadolinium-based nano-particle [28]	Combined MRI with biological targeting [29] and optical detection [26], [29], [30]
	Ironoxide-based nano-particles [31], [32]	
	Multiple-mode imaging contrast nano-agents	
Optical detection	Semiconductor nano-crystals [33]–[36]	Optical detection
	Quantum dots [33]–[36]	
Nano scale field-effect bio-transistor	Silicon nano-wires [37], [38]	Reporting changes in their conductance that are generated by molecular binding events on their surface
Carbon nano-technology	Nano-tubes have been reported as high-specificity sensors of antibody signatures of autoimmune disease [39] and of single-nucleotide polymorphisms (SNPs) [40]	Electronic biosensors
Quantum dot bio-conjugates with targeting	Molecular signatures including ERBB2 [22], [23]	Long-term multiple color imaging, immune-fluorescent labeling
Nano-particle-based methods	Covalently linked antibodies [41], [42]	Confocal microscopy
	Fluorophore-laden silica beads have been used for the identification of leukaemia cells in blood samples [43]	Optical identification
	Fluorescent nanoparticles have been used for an ultrasensitive DNA-detection system [44]	Fluorescence identification

For the second tier of abnormality detection architecture, one may also consider the recent proposals of wireless nano sensor networks; including diffusion-based molecular communication [49], medical imaging techniques [31], ultrasonic communications [50], [51], optical communication using plasmonic nano-antennas [52] and terahertz communication techniques [53].

In this paper, a nano abnormality detection scheme (NADS) is proposed for the detection of nano-scale abnormality in a bio-molecular environment using a two-tier decision-making process. The abnormality is due to the existence of competitor cells in the said environment. The NADS includes a set of SNMs for the detection of a nano-scale abnormality over a nano-communication channel (NCC) with spatially correlated noise. The spatial correlation of noise among SNMs is motivated by the nature of bio-molecular environment in the nano-scale, and as we shall demonstrate highly influences the overall detection performance of the NADS. The SNMs communicate their decisions over a noisy micro-communication channel (MCC) to a data gathering node using micro-scale messages (MSMs). Fusing the collected

TABLE II: List of acronyms

Acronym	Definition
AWGN	Additive white Gaussian noise
AD	Abnormality detection
DGN	Data gathering node
EGFR	Epidermal growth factor receptor
ERBB2	Avian erythroblastosis oncogene B-2
GLRT	Generalized likelihood ratio test
MAP	Maximum a-posteriori probability
MCC	Micro communication channel
MRI	Magnetic resonance imaging
MSM	Micro-scale message
NADS	Nano abnormality detection scheme
NCC	Nano communication channel
PDF	Probability distribution function
SNM	Sensor nano-machine
VTNM	Virtual transmitter nano-machine

signals, the DGN makes a decision and may alarm the presence of an abnormality as necessary. In Table II list of used acronyms in this paper and their definitions are discribed.

The performance analysis of the SNMs over the NCC is set up as a generalized likelihood ratio test, which quantifies the probability of false alarm and the probability of misdetection. Next, incorporating the effect of MCC, the total detection performance of NADS at the DGN is analyzed. The correlated noise in the NCC is assumed Gaussian (similar to [54]–[57]). In this case, the overall NADS detection performance is efficiently approximated and expressed in terms of the performances of the constituent NCCs and MCC. The presented analyses are then used to obtain the optimized concentration of SNMs in the sample for a prescribed high probability of abnormality detection and a bounded false alarm probability. Extensive numerical results are provided to quantify the effect of different design and system parameters on the NADS performance. Specifically, the effects of temporal and spatial correlation of noise at the SNMs on the detection performance are investigated.

The outline of this paper is as follows. In Section II, preliminaries and problem statement are presented. The communication strategy on nano and micro communication channels are described in Section III. In Section IV, the performance of NADS is evaluated analytically. Numerical results are presented in Section V. Finally, conclusions are made in Section VI.

TABLE III: Effective parameters in transition probability of NCC [15]

Parameter	Parameter Description	Unit
θ	Temperature	K
χ	Distance between nano-transmitter and SNM	m
C_R	Concentration of nano receptors, denoted by R , on the SNM	$\mu\text{mol/l}$
C_A	Concentration of Molecular bit A , transmitted by VTNM	$\mu\text{mol}/(\text{l s})$
C_B	Concentration of bind-receptor, denoted by B , on the SNM	$\mu\text{mol}/(\text{l s})$
κ_1	Binding rate	$\mu\text{mol}/(\text{l s})$
κ_{-1}	Release rate	$\mu\text{mol}/(\text{l s})$
κ_0^{-1}	Zero force release	s^{-1}
k_{BC}	Boltzmann Constant	J/K
N_{x_i}	The number of received molecule when the VTNM sends the molecular bit $x_i \in \{A, 0\}$ during time t_{TN} at time i .	$\mu\text{mol/l}$
P_A	Probability of transmission of molecular bit A by the VTNM.	

II. PRELIMINARIES AND PROBLEM STATEMENT

In this Section, the setup of NADS and the problem statement under consideration are described. The NADS comprises of two tiers. In the first tier, each SNM detects the detection feature in nano-scale and emits a micro-scale message [58]. In the second tier, a DGN collects the transmitted MSMs from multiple SNMs.

The NCC models the molecular environment. In the healthy setting, no abnormality (here competitor cell) exists in the molecular environment. The molecular competitor changes the rate of binding between the molecules and the nano-receptors on the SNM or changes the number of transmitted molecules by the so-called virtual transmitter nano-machine (VTNM). This is reflected in the NCC model, with the VTNM as the transmitter and the SNMs as the receivers.

Each of the SNMs generate an MSM as it detects an abnormality. The DGN collects the MSMs over a noisy micro-communication channel. Then it decides, and declares the presence or the absence of the abnormality to the outside world. The MCC is considered an additive white Gaussian noise (AWGN) channel. Below, we continue with a detailed description of the NCC model and the detection feature.

A. Nano Communication Channel

The NCC characterizes chemical reactions in the molecular environment. We consider a set of SNMs, which act as molecular receivers, injected into the biological tissue for test. We assume that the existing molecules in the molecular environment react with the receptors on SNMs. The molecules are assumed to be transmitted by a VTNM with a periodic square pulse propagation pattern. A molecular pulse A (or 0)

is emitted by VTNM as x_i , $x_i \in \{A, 0\}$, with concentration C_A (or 0) and probability P_A (or $(1 - P_A)$), during time $it_{TN} \leq t \leq (i+1)t_{TN}$, $i = 0, 1, \dots$, where t_{TN} is the duration of the pulses transmitted by VTNM [59]. The transmitted molecules are absorbed at the sensor nano-machine. If the VTNM transmits a molecular pulse A , the number of received molecules during the time t_{TN} is quantified by

$$N_A = \int_0^{t_{TN}} C_B(t) dt, \quad (1)$$

in which $C_B(t)$ denotes the concentration of the bound receptors, in terms of $\mu\text{mol/liter}$ and is given by

$$C_B(t) = C_B(\infty) \left(1 - e^{-t(\kappa_{-1} + \kappa_1 C_A)}\right), 0 \leq t \leq t_{TN}, \quad (2)$$

where $C_B(\infty) = \kappa_1 C_A C_R / (\kappa_{-1} + \kappa_1 C_A)$ is the steady state concentration of the bound receptors [15].

The parameters κ_1 and κ_{-1} , respectively are binding and release rates for the following reactions



where R and B respectively, denote nano-receptors on the SNMs and the bound-receptors after reaction between A and R . It is evident in (2) that $C_B(t)$ is increased exponentially over time within the pulse period with concentration of C_A . After time t_{TN} , when the pulse duration ends, $C_B(t)$ is reduced as

$$C_B(t) = C_B(t_{TN}) \exp(-\kappa_{-1}(t - t_{TN})) \text{ for } t > t_{TN}. \quad (4)$$

As a result, at the SNM and over the subsequent time interval, this previous pulse is reflected as follows in the receiver

$$N'_A = \int_0^{t_{TN}} N_A e^{(-\kappa_{-1}t)} dt. \quad (5)$$

Obviously, we have $N_0 = N'_0 = 0$. The rates of interaction of the molecules with the SNM receptors, κ_1 and κ_{-1} , depend on the molecular diffusion over the NCC. Hence, κ_1 may be influenced by such parameters as the molecular diffusion coefficient and the temperature of the environment, θ [60], and may be assessed analytically [61]. The release rate, κ_{-1} is given by [60]

$$\kappa_{-1} = \kappa_{-1}^0 e^{\chi v / k_{BC} \theta}, \quad (6)$$

in which v depends on the energy of the molecules propagated between the VTNM and the SNMs and environment factors, and χ , k_{BC} and θ are defined in Table III. The parameter κ_{-1}^0 can be obtained by matching experimental measurements, and depends on the absorption capability of molecules at the SNM [60]. Hence, it is assumed that κ_{-1}^0 is a variable, which depends on the properties of nano-receptors in the SNM.

The noise of the SNM measurement is correlated over time and space. The former is due to the slow variation of SNM measurement as it models a bio-chemical reaction. The latter is due to the relatively small volume of the molecular environment in the range of nm^3 to μm^3 . The NCC is modeled by a first order Markov model with additive noise, and as such the input of SNM j at time i is described by

$$y_{ij} = g^+(x_i, \kappa_1, \kappa_{-1}, t_{TN}, C_A, \theta) + g^-(x_{i-1}, \kappa_1, \kappa_{-1}, t_{TN}, C_A, \theta) + \varepsilon_{ij}. \quad (7)$$

In (7), if the VTNM transmits the molecular bit $x_i \in \{A, 0\}$, then

$$g^+(x_i, \kappa_1, \kappa_{-1}, t_{TN}, C_A, \theta) = N_{x_i}, \quad (8)$$

$$g^-(x_{i-1}, \kappa_1, \kappa_{-1}, t_{TN}, C_A, \theta) = N'_{x_{i-1}}, \quad (9)$$

indicate the number of molecules received in the current time interval from the current and previous transmissions, respectively. Also, ε_{ij} 's are jointly normal distributed with an assumed time correlation span of p . The temporal (normalized) covariance matrix of ε_{ij} 's is given by

$$\Omega^{TC} = [\omega_{ij}^{TC}]_{p \times p}. \quad (10)$$

The SNM observes the nano-communications channel for a time duration of $n \geq p$. We next consider the spatial correlation. The spatial (normalized) covariance matrix of SNM noises ε_{ij} is given by

$$\Omega^{SC} = [\omega_{jl}^{SC}]_{M \times M}, \quad (11)$$

in which M is the number of SNMs, ω_{jl}^{SC} is the correlation coefficient of observations of SNMs j and l . Moreover, in this paper we assume that the space-time correlation function of SNM noises is

separable [62], [63]. As such, the correlation coefficient of ε_{ij} and ε_{kl} is given by

$$\frac{E(\varepsilon_{ij}\varepsilon_{kl})}{\sqrt{E(\varepsilon_{ij}^2)E(\varepsilon_{kl}^2)}} = \omega_{ik}^{TC} \omega_{jl}^{SC}. \quad (12)$$

The Gaussian NCC model we consider here is also justified from a molecular communication perspective. The propagation models of molecules over a diffusive molecular communication channel are widely studied in the literature [17], [64]–[68]. In a molecular communication system, with information encoded in the number of molecules, the number of received molecules exhibits a binomial process [68]. When multiple emissions are considered, due to the ISI caused by the diffusion channel, previous transmissions must also be taken into account for the determination of the current symbol. This requires a summation of the binomial random variables, which is analytically hard to work with. Therefore, in the literature, two approximations of the binomial distribution are used, namely the Poisson and Gaussian approximations [67], [69]–[71]. In [72], it is shown that when the number of transmitted molecules increases, the Gaussian approximation provides a good model for the molecular communications channel.

B. Detection Feature

The biochemical activities of the competitor cells, e.g., cancer cells, affect the molecular environment and change its parameters [18]. We model this as an abnormality or intrusion in the molecular environment, which is to be detected as early as possible. The presence of competitor cells affects the NCC. For example, the competitor cells can react with the molecules transmitted by the VTNM. This reduces the concentration of transmitted molecules C_A , and hence, changes the NCC parameters or input. This variation in NCC parameters or input is used for modeling of protein identification for early cancer detection in the nano-scale [18]. Alternatively, the competitor cells may devitalize the receptors on the SNMs, change κ_{-1} and κ_1 on the SNM by a biochemical reaction or vary the temperature of nano-receptors on the SNMs.

In the NCC, for a given size of sample tissue and the parameters in Table III, a measurable parameter is defined as detection feature, which is to be constant during measurement. In presence of competitor cells, this parameter deviates from its normal value, that in turn is detected by the SNM. Here, we consider two scenarios although other scenarios may also be similarly considered. In the first scenario, we assume that the VTNM always sends molecular bit 0 ($P_A = 0$) in the healthy setting, and sends only molecular

bit A ($P_A = 1$) when an abnormality exists. In this case, the detection feature is defined as follows

$$NR = g^+(x_i, \kappa_1, \kappa_{-1}, t_{TN}, C_A, \theta) + g^-(x_{i-1}, \kappa_1, \kappa_{-1}, t_{TN}, C_A, \theta). \quad (13)$$

Hence, NR in (13) is a constant value in the healthy setting and changes to another constant value as the environmental parameters vary in the non-healthy setting.

In the second scenario, we assume that VTNM sends molecular bit A with probability P_A and the presence of a competitor cell in the environment can change P_A and/or channel parameters. In this case, NR in (13) is not a constant value over multiple transmissions, but its average is still so. As such, the detection feature is defined as follows

$$NR = E(g^+(x_i, \kappa_1, \kappa_{-1}, t_{TN}, C_A, \theta) + g^-(x_{i-1}, \kappa_1, \kappa_{-1}, t_{TN}, C_A, \theta)), \quad (14)$$

where, the expectation (average) at the receiver is naturally computed over multiple transmission time slots, t_{TN} . By this definition, NR in (14) has two distinct constant values in the healthy and non-healthy settings, and is used as an abnormality detection feature. In this case, we rewrite (7), with a new channel output interpretation, as follows (this allows us to treat both scenarios in a common setting in the sequel)

$$y_{ij} = E(g^+(x_i, \kappa_1, \kappa_{-1}, t_{TN}, C_A, \theta) + g^-(x_{i-1}, \kappa_1, \kappa_{-1}, t_{TN}, C_A, \theta)) + \varepsilon_{ij}. \quad (15)$$

Note that the same Gaussian model described in (10)-(12) for ε_{ij} is adopted here. Obviously the model parameters may not be necessarily the same in the two mentioned scenarios. It is noteworthy that the separability of the space-time correlation function remains valid.

In both noted scenarios, the NCC is considered homogeneous and we have $E[(y_{ij} - NR)^2] = E[(y_{il} - NR)^2]$, $j, l \in \{1, \dots, M\}$ and $i \in \{1, \dots, n\}$. In the healthy setting, $NR = NH$; and in presence of a competitor cell or an abnormality that affects the NCC parameters or input, NR deviates from NH . In the sequel, we consider y_{ij} as a decision variable, whose time average NR serves as a detection feature for abnormality detection at SNM j .

C. Problem Statement

We consider a design optimization problem to determine the minimum required concentration of SNMs, $\bar{M} = M/vol$, in the test environment for a reliable NADS, where vol is the volume of the sample.

The SNMs are typically synthesized chemical compounds that could be expensive or could create side effects if used in vivo. Hence, we wish to use them in the smallest concentration possible. A reliable NADS would identify the existence of an abnormality with sufficiently high probability, P_D . At the same time, when the abnormality in fact does not exist it only makes a (false) alarm with sufficiently small probability, P_F . The P_D and P_F are later analyzed in Theorem 3. The desired optimization problem in this paper is formulated as follows.

Problem. The NADS design optimization problem is given by

$$\begin{aligned} \bar{M}^* &= \min \bar{M} \\ \text{subject to } P_D &\geq \xi, P_F \leq \gamma. \end{aligned} \tag{16}$$

where, ξ is a constant close to unity and γ is a constant close to zero. As observed in Section V for given values of ξ and γ , the optimized concentration of SNMs, \bar{M} , depends on type or level of abnormality, k .

III. DETECTION STRATEGY OVER NCC AND MCC

In this Section, the detection strategy over NCC and MCC is studied. In the first Subsection, a hypothesis test is set up for the detection of competitor cells in the bio-molecular environment. Subsequently, the communication and detection strategies over the MCC are studied.

A. Hypothesis Test for AD in NCC

This test determines the functionality of the SNM over the NCC. We derive a threshold level for each SNM to alarm the presence of competitor cells by generating a micro scale message. This is accomplished such that the detection probability of each SNM over the NCC is maximized for a bounded probability of false alarm. The detection probability in terms of the false alarm probability is the basic performance characteristic of an SNM over the NCC.

The following hypothesis test is considered for the detection of a competitor cell in the molecular environment

$$\begin{cases} H_0, & NR = NH \\ H_1, & NR \neq NH. \end{cases} \tag{17}$$

The Gaussian assumption for the observation is motivated based on thermal noise distribution, the noise in gene expression levels [55] and the noise of biochemical systems [57]. In the sequel, the detection

performance of the hypothesis test in (17) is analyzed, where we consider maximum likelihood estimate of NR at the SNM over the observation period n , i.e., $\widehat{NR}_j = \arg \max_{NR} P(\mathbf{y}_j^n | NR)$, where $\mathbf{y}_j^n = [y_{1j}, y_{2j}, \dots, y_{nj}]^\dagger$, where \dagger denotes the transpose operation. If we rewrite (7) and (15) at the receiver in terms of NR , respectively based on definition of NR in (13) or (14), for SNM $j = 1, 2, \dots, M$ and time $i = 1, 2, \dots, n$, we have

$$y_{ij} = NR + \varepsilon_{ij}. \quad (18)$$

Without loss of generality, we consider $n \geq p$, and define the extended temporal (normalized) covariance matrix of observations within the observation period n as follows

$$\Omega^T = [\omega_{ij}^{TC}]_{n \times n} = \begin{bmatrix} \Omega^{TC} & \dots & \underline{0} \\ \vdots & \ddots & \vdots \\ \underline{0} & \dots & \Omega^{TC} \end{bmatrix}_{n \times n}. \quad (19)$$

For example with $p = 2$ and $\omega_{12}^{TC} = \omega_{21}^{TC} = \rho$, Ω^T is given by

$$\Omega^T = \begin{bmatrix} 1 & \rho & \dots & 0 \\ \rho & 1 & \dots & 0 \\ \vdots & \vdots & \ddots & \vdots \\ 0 & 0 & \rho & 1 \end{bmatrix}_{n \times n}. \quad (20)$$

By this model of channel, as the status of the molecular environment departs from a healthy setting, the detection feature, NR , deviates from NH . Here, NR deviates from NH as follows

$$NR = (1 \pm k\sigma_{NCC}) NH, \quad (21)$$

in which k could indicate the type or level of abnormality and σ_{NCC} is standard deviation of noise in NCC. For $k = 0$, the molecular environment is healthy ($NR = NH$) and we assume $1 \pm k\sigma_{NCC} \geq 0$, $k \geq 0$. A certain value of k could correspond to a given progress level of a disease.

The conditional probability of observations vector \mathbf{y}_j^n , given NR at SNM j is computed as follows,

where \dagger denotes the transpose operation,

$$P(\mathbf{y}_j^n | NR) = P(y_{1j}, y_{2j}, \dots, y_{nj} | NR) = \frac{1}{(2\pi)^{n/2} \sigma_{NCC}^n |\Omega^T|^{1/2}} \exp\left(-\frac{1}{2\sigma_{NCC}^2} (\mathbf{y}_j^n - \mathbf{NR}^n)^\dagger \Omega^{T^{-1}} (\mathbf{y}_j^n - \mathbf{NR}^n)\right). \quad (22)$$

and $\mathbf{NR}^n = \begin{bmatrix} NR & NR & \dots & NR \end{bmatrix}_{n \times 1}^\dagger$. Considering the Logarithm of (22), we have

$$\log P(\mathbf{y}_j^n | NR) = -n \log\left(|\Omega^T|^{1/(2n)} \sqrt{2\pi\sigma_{NCC}^2}\right) - \frac{1}{2\sigma_{NCC}^2} (\mathbf{y}_j^n - \mathbf{NR}^n)^\dagger \Omega^{T^{-1}} (\mathbf{y}_j^n - \mathbf{NR}^n). \quad (23)$$

We define

$$\Psi^T = [\psi_{ij}^{TC}]_{n \times n} \triangleq \Omega^{T^{-1}}, \quad (24)$$

and rewrite (23) as follows

$$\log P(\mathbf{y}_j^n | NR) = -n \log\left(|\Omega^T|^{1/(2n)} \sqrt{2\pi\sigma_{NCC}^2}\right) - \frac{1}{2\sigma_{NCC}^2} \sum_{l=1}^n \sum_{i=1}^n (y_{lj} - NR) (y_{ij} - NR) \psi_{il}^{TC}. \quad (25)$$

To maximize (23), we set its derivative with respect to NR to zero and considering the symmetry of Ω^T obtain

$$\widehat{NR}_j = \frac{\sum_{l=1}^n \sum_{i=1}^n y_{lj} \psi_{il}^{TC}}{\sum_{l=1}^n \sum_{i=1}^n \psi_{il}^{TC}} \quad (26)$$

To derive the decision rule of Neyman-Pearson as in the hypothesis test of (17), we employ the generalized likelihood ratio test (GLRT) in the next theorem due to the hypothesis test in (17) is composite test [73].

Theorem 1. Consider an SNM with n temporally correlated Gaussian observations over the NCC. For the hypothesis test in (17), the decision threshold and the detection probability with limited probability of false alarm, $P_F^{NCC} < \eta_1$, are given by

$$\begin{cases} H_0, & NH - \sigma_D \phi^{-1}\left(1 - \frac{\eta_1}{2}\right) < \widehat{NR}_j < NH + \sigma_D \phi^{-1}\left(1 - \frac{\eta_1}{2}\right) \\ H_1, & \begin{aligned} & \widehat{NR}_j > NH + \sigma_D \phi^{-1}\left(1 - \frac{\eta_1}{2}\right) \\ & \widehat{NR}_j < NH - \sigma_D \phi^{-1}\left(1 - \frac{\eta_1}{2}\right), \end{aligned} \end{cases} \quad (27)$$

$$P_D^{NCC} = 1 - \mathcal{Q}\left(\frac{-\sigma_D \phi^{-1}\left(1 - \frac{\eta_1}{2}\right) \mp k\sigma_{NCC} NH}{\sigma_D}\right) + \mathcal{Q}\left(\frac{\sigma_D \phi^{-1}\left(1 - \frac{\eta_1}{2}\right) \mp k\sigma_{NCC} NH}{\sigma_D}\right), \quad (28)$$

where $\phi^{-1}(\cdot)$ is the inverse function of normal cumulative distribution, ϕ ; $\mathcal{Q}(\cdot) = 1 - \phi(\cdot)$ is Q-functions

and

$$\sigma_D = \sqrt{\left(\sum_{l=1}^n \sum_{i=1}^n \psi_{il}^{TC} \right)^{-2} \left\{ \sum_{l=1}^n \left(\sum_{i=1}^n \psi_{il}^{TC} \right)^2 \sigma_{NCC}^2 + 2 \sum_{l=1}^{n-1} \sum_{q=l+1}^n \omega_{kl}^{TC} \sigma_{NCC}^2 \left(\sum_{i=1}^n \psi_{iq}^{TC} \right) \left(\sum_{i=1}^n \psi_{il}^{TC} \right) \right\}}$$

Proof. See Appendix A.

The probability of miss-detection for each SNM then is given by

$$P_M^{NCC} = 1 - P_D^{NCC}. \quad (29)$$

As we shall demonstrate in Section V, a larger n would enhance the performance in general. However, the level of obtained gain depends on the temporal dependency of the SNM observations. In the next Section, we study the abnormality detection and communication over the MCC.

B. Detection and Communication Strategy over MCC

The DGN receives the MSMs from the SNMs over the MCC and declares either the existence or the absence of the competitor cells in the NCC. It is assumed that the MSMs have two alphabets. If the SNM j detects the competitor cells, it generates the message $X_j = G$, otherwise it sets $X_j = 0$. Replacing (26) in the decision rule of SNM j in (27), we have

$$X_j = \begin{cases} 0, & NH - \sigma_D \phi^{-1} \left(1 - \frac{\eta_1}{2}\right) < \sum_{l=1}^n \sum_{i=1}^n y_{lj} \psi_{il}^{TC} / \sum_{l=1}^n \sum_{i=1}^n \psi_{il}^{TC} < NH + \sigma_D \phi^{-1} \left(1 - \frac{\eta_1}{2}\right) \\ G, & \begin{aligned} & \sum_{l=1}^n \sum_{i=1}^n y_{lj} \psi_{il}^{TC} / \sum_{l=1}^n \sum_{i=1}^n \psi_{il}^{TC} > NH + \sigma_D \phi^{-1} \left(1 - \frac{\eta_1}{2}\right) \\ & \sum_{l=1}^n \sum_{i=1}^n y_{lj} \psi_{il}^{TC} / \sum_{l=1}^n \sum_{i=1}^n \psi_{il}^{TC} < NH - \sigma_D \phi^{-1} \left(1 - \frac{\eta_1}{2}\right), \end{aligned} \end{cases} \quad (30)$$

The probability of the events $X_j = G$ and $X_j = 0$ depends on the presence or the absence of the competitor cell. If the competitor cell is present in the molecular environment, the probability of micro-scale message is given by

$$p(X_j | NR \neq NH) = \begin{cases} 1 - P_D^{NCC} & X_j = 0 \\ P_D^{NCC} & X_j = G. \end{cases} \quad (31)$$

If the competitor cell is not present in the environment the probability of micro-scale message is given by

$$p(X_j | NR = NH) = \begin{cases} 1 - P_F^{NCC} & X_j = 0 \\ P_F^{NCC} & X_j = G, \end{cases} \quad (32)$$

The signal received at the DGN through the AWGN MCC then is given by

$$V = \sum_{j=1}^M X_j + \varepsilon_{DGN}, \quad (33)$$

where, $\varepsilon_{DGN} \sim \mathcal{N}(0, \sigma_{MCC}^2)$, and σ_{MCC}^2 is the MCC noise variance. We set up the following hypothesis test at the DGN,

$$\begin{cases} H_0 & \sum_{j=1}^M X_j < G \\ H_1 & \sum_{j=1}^M X_j \geq G. \end{cases} \quad (34)$$

This fusion rule is known as the OR-rule [74]. The hypothesis $H_1(H_0)$ is declared if at least one (none) of the SNMs transmits the MSM G , stating that the abnormality exists (does not exist) in the bio-molecular environment. In the next Section, the NADS performance is analyzed when the SNMs observations are spatially, and temporally correlated.

IV. NADS PERFORMANCE ANALYSIS

In this Section, the performance of NADS is analyzed and two closed-form expressions for the probabilities of detection and false alarm are derived. Then, in the next Subsection, a computationally efficient formulae is derived for performance of NADS.

A. Exact Performance Analysis

In this Subsection, the NADS performance is quantified using *Theorem 1* on the NCC performance and considering the communication of SNMs over the MCC as discussed in Section III. Fig. 1 shows the modeling of the communication channels between the VTNM, the SNMs and the DGN. The NADS is composed of a broadcast channel with a common message followed by a Gaussian multiple access channel and an OR fusion rule.

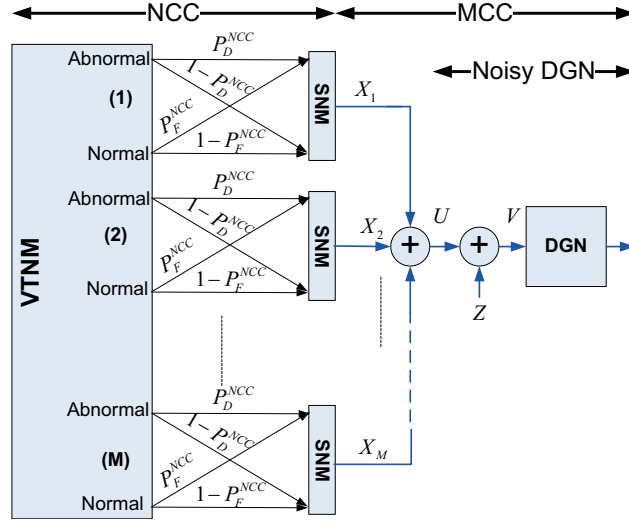


Fig. 1: Modeling of communication channels between VTNM, SNMs and the DGN.

Considering Fig. 1 and the communication of SNMs over the MCC, we have

$$U = \sum_{j=1}^M X_j. \quad (35)$$

The event of abnormality detection alarm at the SNM j , when the abnormality truly exists, is denoted by D_j and its complementary event is denoted by D'_j . In this case, we consider $Q_D = P(U \geq G | NR \neq NH)$. Considering the spatially correlated observations of SNMs and using the OR-fusion rule, Q_D can be written as follows

$$Q_D = 1 - \Pr \left\{ \bigcap_{j=1}^M D'_j \right\}. \quad (36)$$

The SNM j alarms an abnormality over the NCC depending on its decision variable \widehat{NR}_j in (26). Hence, to quantify the probability in (36), we need to derive the PDF of $\widehat{\mathbf{NR}}^M = [\widehat{NR}_1 \ \widehat{NR}_2 \ \dots \ \widehat{NR}_M]^\dagger$. The next lemma serves this purpose.

Lemma 1. The decision variables of SNMs $\widehat{\mathbf{NR}}^M = [\widehat{NR}_1 \ \widehat{NR}_2 \ \dots \ \widehat{NR}_M]^\dagger$ are jointly Gaussian with mean NR and (normalized) covariance matrix Ω^{SC} in (11).

Proof. See Appendix B.

Using *Lemma 1* and noting the decision region in (27), we have

$$Q_D = 1 - \int_{NH-\tau'}^{NH+\tau'} \dots \int_{NH-\tau'}^{NH+\tau'} \frac{1}{(2\pi)^{M/2} \sigma_D^M |\Omega^{SC}|^{1/2}} \exp \left(-\frac{1}{2\sigma_D^2} \left(\widehat{\mathbf{NR}}^M - \mathbf{NR}^M \right)^\dagger \Omega^{SC^{-1}} \left(\widehat{\mathbf{NR}}^M - \mathbf{NR}^M \right) \right) d\widehat{NR}_1 \dots d\widehat{NR}_M \quad (37)$$

where $\mathbf{NR}^M = \begin{bmatrix} NR & NR & \dots & NR \end{bmatrix}_{1 \times M}$. In a similar manner, we consider E_j as the false alarm event that SNM j alarms an abnormality, when it does not exist in reality. The complementary event is denoted by E'_j . In this case, we consider $Q_F = P(U \geq G | NR = NH)$. Considering the spatially correlated observations of SNMs and using the OR-fusion rule, Q_F can be rewritten as follows

$$Q_F = 1 - \Pr \left\{ \bigcap_{j=1}^M E'_j \right\} \quad (38)$$

Using *Lemma 1* and noting the decision region in (27), we have

$$Q_F = 1 - \int_{NH-\tau'}^{NH+\tau'} \dots \int_{NH-\tau'}^{NH+\tau'} \frac{1}{(2\pi)^{M/2} \sigma_D^M |\Omega^{SC}|^{1/2}} \exp \left(-\frac{1}{2\sigma_D^2} \left(\widehat{\mathbf{NR}}^M - \mathbf{NH}^M \right)^\dagger \Omega^{SC^{-1}} \left(\widehat{\mathbf{NR}}^M - \mathbf{NH}^M \right) \right) d\widehat{NR}_1 \dots d\widehat{NR}_M \quad (39)$$

where $\mathbf{NH}^M = \begin{bmatrix} NH & NH & \dots & NH \end{bmatrix}_{1 \times M}$. If the observations of different SNMs are spatially independent, Ω^{SC} is diagonal and (37) and (39) are simplified as follows [74],

$$Q_D = 1 - (1 - P_D^{NCC})^M \quad (40)$$

$$Q_F = 1 - (1 - P_F^{NCC})^M \quad (41)$$

where $P_F^{NCC} = \eta_1$ and P_M^{NCC} is defined in (29).

At the DGN with the OR-rule, we are facing a channel with binary outputs. However, the input to the DGN is a noisy version of U , i.e., V , which is the basis for the decision on the possible presence of abnormality. The next theorem presents the corresponding decision region at the DGN based on maximum a-posteriori probability (MAP) rule. This is motivated to obtain a point estimate of the unobserved quantity of presence or non-presence of abnormality based on DGN observations.

Theorem 2. The decision region at the DGN based on MAP rule is given by

$$\begin{cases} H_0 : V < V^{THR} \\ H_1 : V > V^{THR} \end{cases} \quad (42)$$

where, V^{THR} is the minimum value of V , satisfying the following inequality,

$$\begin{aligned} & ((1 - Q_F) P(H_0) - (1 - Q_D) P(H_1)) \exp \left(\frac{-V^2}{2\sigma_{MCC}^2} \right) + \\ & (Q_F P(H_0) - Q_D P(H_1)) \frac{1}{(1-p_0)} \sum_{l=1}^M p_l \exp \left(\frac{-(V-lG)^2}{2\sigma_{MCC}^2} \right) \stackrel{H_0}{\underset{H_1}{>}} 0. \end{aligned} \quad (43)$$

In (43), $p_l = \Pr \{U = lG\}$ for $l \in \{0, \dots, M\}$, is given by

$$p_l = P(H_1)p'_l + P(H_0)p''_l \quad (44)$$

where p'_l and p''_l are given by

$$p'_l = \Pr\{U = lG | H_1\} = \binom{M}{l} \underbrace{\int_A \dots \int_A}_l \underbrace{\int_{A^c} \dots \int_{A^c}}_{M-l} \quad (45)$$

$$\frac{1}{(2\pi)^{M/2} \sigma_D^M |\Omega^{SC}|^{1/2}} \exp\left(-\frac{1}{2\sigma_D^2} \left(\widehat{\mathbf{NR}}^M - \mathbf{NR}^M\right)^\dagger \Omega^{SC^{-1}} \left(\widehat{\mathbf{NR}}^M - \mathbf{NR}^M\right)\right) d\widehat{NR}_1 \dots d\widehat{NR}_M$$

$$p''_l = \Pr\{U = lG | H_0\} = \binom{M}{l} \underbrace{\int_A \dots \int_A}_l \underbrace{\int_{A^c} \dots \int_{A^c}}_{M-l} \quad (46)$$

$$\frac{1}{(2\pi)^{M/2} \sigma_D^M |\Omega^{SC}|^{1/2}} \exp\left(-\frac{1}{2\sigma_D^2} \left(\widehat{\mathbf{NR}}^M - \mathbf{NH}^M\right)^\dagger \Omega^{SC^{-1}} \left(\widehat{\mathbf{NR}}^M - \mathbf{NH}^M\right)\right) d\widehat{NR}_1 \dots d\widehat{NR}_M.$$

$$\int_A \bullet = \int_{-\infty}^{NH-\tau'} \bullet + \int_{NH+\tau'}^{\infty} \bullet \quad \text{and} \quad \int_{A^c} \bullet = \int_{NH-\tau'}^{NH+\tau'} \bullet,$$

Proof. See Appendix C.

Hence, the next theorem quantifies the NADS performance.

Theorem 3. The probabilities of detection and false alarm of NADS are given by

$$P_D = \mathcal{Q}\left(\frac{V^{THR}}{\sigma_{MCC}}\right) (1 - Q_D) + \frac{\sum_{l=1}^M \mathcal{Q}\left(\frac{V^{THR}-lG}{\sigma_{MCC}}\right) p'_l}{1 - p'_0} Q_D \quad (47)$$

$$P_F = \mathcal{Q}\left(\frac{V^{THR}}{\sigma_{MCC}}\right) (1 - Q_F) + \frac{\sum_{l=1}^M \mathcal{Q}\left(\frac{V^{THR}-lG}{\sigma_{MCC}}\right) p''_l}{1 - p''_0} Q_F \quad (48)$$

Proof. The proof is provided in Appendix D.

If the noise of SNMs are considered spatially independent, the next corollary presents the NADS probability of detection and false alarm.

Corollary 1. The probability of detection and false alarm of NADS for spatially independent NCCs are given by

$$P_D = \mathcal{Q}\left(\frac{V^{THR}}{\sigma_{MCC}}\right) (1 - P_D^{NCC})^M + \frac{\sum_{l=1}^M \mathcal{Q}\left(\frac{V^{THR}-lG}{\sigma_{MCC}}\right) p'_l}{1 - p'_0} \left(1 - (1 - P_D^{NCC})^M\right) \quad (49)$$

$$P_F = \mathcal{Q}\left(\frac{V^{THR}}{\sigma_{MCC}}\right) (1 - P_F^{NCC})^M + \frac{\sum_{l=1}^M \mathcal{Q}\left(\frac{V^{THR}-lG}{\sigma_{MCC}}\right) p''_l}{1 - p''_0} \left(1 - (1 - P_F^{NCC})^M\right) \quad (50)$$

where

$$p'_l = \binom{M}{l} (1 - P_D^{NCC})^{M-l} (P_D^{NCC})^l \quad (51)$$

$$p''_l = \binom{M}{l} (1 - P_F^{NCC})^{M-l} (P_F^{NCC})^l. \quad (52)$$

Remark. 1. The analysis in Theorem 3 relies on an OR rule (1 out of M rule). This can be extended to the case with m out of M rule at the DGN. Specifically, following similar steps, it is straight forward to show that the probabilities of detection and false alarm are given by

$$P_D = \sum_{l=0}^M p'_l \mathcal{Q} \left(\frac{V^{THR} - lG}{\sigma_{MCC}} \right) \quad (53)$$

$$P_F = \sum_{l=0}^M p''_l \mathcal{Q} \left(\frac{V^{THR} - lG}{\sigma_{MCC}} \right). \quad (54)$$

where V^{THR} is smallest value of V which satisfy the next inequality

$$\begin{aligned} & \frac{((1 - \check{Q}_F) P(H_0) - (1 - \check{Q}_D) P(H_1))}{\sqrt{2\pi\sigma_{MCC}^2} \sum_{l=0}^{m-1} p_l} \sum_{l=0}^{m-1} p_l \exp \left(-\frac{(V - lG)^2}{2\sigma_{MCC}^2} \right) + \\ & \frac{(\check{Q}_F P(H_0) - \check{Q}_D P(H_1))}{\sqrt{2\pi\sigma_{MCC}^2} \sum_{l=k}^M p_l} \sum_{l=m}^M p_l \exp \left(-\frac{(V - lG)^2}{2\sigma_{MCC}^2} \right) \stackrel{H_0}{\geq} 0 \end{aligned} \quad (55)$$

where $\check{Q}_D = \sum_{l=m}^M p'_l$ and $\check{Q}_F = \sum_{l=m}^M p''_l$. It is obvious that V^{THR} explicitly depends on m . Indeed, for the case of $m = 1$ replacing Q_D and Q_F in terms of p'_l and p''_l in (45) and (46) leads to (53) and (54). Our experiments (not reported here) reveal that both P_D and P_F reduce as m increases beyond one. Assuming SNMs have small P_F^{NCC} and P_D^{NCC} , and considering our application of early disease detection, in the sequel we focus on the 1 out of M rule and aim at improving the probability of detection, with a small and acceptable probability of false alarm. As elaborated, similar analysis can be carried out for the case of m out of M rule.

B. Computationally Efficient Performance Assessment

Performance evaluation of NADS based on the analyses in Theorem 2 and equations (44), (45) and (46) is computationally challenging in general, due to the multiple nested integrals involved (especially for

large number of SNMs). Therefore, in the next lemma we present approximations that enable more computationally efficient solutions.

Lemma 2. The probabilities p'_l , p''_l and p_l in (44), (45) and (46) are approximated by

$$p'_l \approx \binom{M}{l} (1 - P_D^{NCC})^{\alpha \frac{M-l}{M}} ([\mathbf{1}]^\dagger \Omega^{SC^{-1}} [\mathbf{1}]) (P_D^{NCC})^{\frac{\alpha l}{M}} ([\mathbf{1}]^\dagger \Omega^{SC^{-1}} [\mathbf{1}]), \quad (56)$$

$$p''_l \approx \binom{M}{l} (1 - P_F^{NCC})^{\alpha \frac{M-l}{M}} ([\mathbf{1}]^\dagger \Omega^{SC^{-1}} [\mathbf{1}]) (P_F^{NCC})^{\frac{\alpha l}{M}} ([\mathbf{1}]^\dagger \Omega^{SC^{-1}} [\mathbf{1}]), \quad (57)$$

$$\tilde{p}_l = P(H_1) \tilde{p}'_l + P(H_0) \tilde{p}''_l. \quad (58)$$

where $[\mathbf{1}] = [1, \dots, 1]_{M \times 1}^\dagger$ and α is a fitting parameter.

Proof. The proof is provided in Appendix E.

Since the DGN uses an OR-fusion rule, we have $Q_D = 1 - p'_0$ and $Q_F = 1 - p''_0$. Using (56) and (57) with $l = 0$, we can approximate Q_D and Q_F in (37) and (39) for their efficient computation as follows:

$$\tilde{Q}_D = 1 - (1 - P_D^{NCC})^{\alpha [\mathbf{1}]^\dagger \Omega^{SC^{-1}} [\mathbf{1}]} \quad (59)$$

$$\tilde{Q}_F = 1 - (1 - P_F^{NCC})^{\alpha [\mathbf{1}]^\dagger \Omega^{SC^{-1}} [\mathbf{1}]} \quad (60)$$

Using the results of Lemma 2 and Corollary 1, computationally efficient expressions for P_D and P_F are obtained by replacing p_l , p'_l , p''_l , Q_D and Q_F with \tilde{p}_l , \tilde{p}'_l , \tilde{p}''_l , \tilde{Q}_D and \tilde{Q}_F , respectively.

V. NUMERICAL RESULTS

In this Section, we present numerical results and assess the performance of the proposed NADS. In addition, the effects of different parameters including the temporal and spatial correlations of the SNM noise are studied. In the experiments of this Section, we assume that the observations of SNMs are temporally correlated by the correlation matrix in (20) and the spatial correlation matrix is $\Omega^{SC} = [\omega_{ij}^{SC}]_{M \times M}$, and $\omega_{ij}^{SC} = (1/4)^{|i-j|}$. We also consider the volume of the sample size at 1000 nm^3 . Table IV presents the parameters of the numerical experiments.

Fig. 2 shows the probability of receiving no microscale messages at the DGN for spatially correlated noise of SNMs in presence of abnormality (in (45)) and its approximation (p'_0 in (56)) in terms of the

number of SNMs, M , for different values of observation time, n . As evident the approximate expression \tilde{p}'_0 matches the analysis p'_0 reasonably well for the selected $\alpha = 1.2$. As such in the subsequent numerical results, we set $\alpha = 1.2$ when using the approximations.

Table V explains the presentation of numerical results in Figs 3a- 5d. Two methods for obtaining the performance results are considered, which are labeled as approximate and numerical in the sequel. First, we elaborate the results and comment on how the two methods are compared. Fig. 3a shows the probability of miss-detection, P_M in terms of the number of SNMs in the sample size, M for different values of observation time, n and temporal correlation ρ in spatially independent scenario. It is evident that even a small value of temporal correlation, e.g., $\rho = 0.1$, greatly affects P_M . Fig. 3b shows P_M in terms of M , for different values of observation time, n in spatially correlated and temporally independent scenario. One sees that spatial correlation of SNM observations degrades P_M . For example, with $M = 8$ and $n = 9$, spatially independent SNM observations results in a 20 times smaller P_M when compared to the spatially correlated setting. Hence, if observations of SNMs are spatially correlated and we consider them as spatially independent, the reliability of NADS is substantially degraded. Figs 3c and 3d show P_M with $\sigma_{MCC} = 0.1$ and $\sigma_{MCC} = 0.4$ in terms of M for different values of n and ρ in spatially and temporally correlated scenario. One sees that increasing σ_{MCC} degrades P_M . Based on results in Figs 3a- 3d, it is evident that the probability of miss-detection P_M obtained by the approximate method matches well with that computed based on the numerical method. Hence, the approximate method can be efficiently used to solve the design problem of (16).

Fig. 4a shows the probability of false alarm P_F in terms of M , for different values of σ_{MCC} . One sees that the behavior of P_F in terms of M varies as σ_{MCC} increases. For small values of σ_{MCC} , the performance degradation is due to error in the NCC. As evident in (50), this performance result is valid for all values of n and ρ , since in this experiment, P_F^{NCC} is small (set to equality in (71)) and σ_{MCC} is also small (effect of MCC is negligible on P_F). Moreover, one sees that any spatial or temporal correlation in SNM observations improves P_F . Fig. 4b shows P_F in terms of M for different values of n with $\sigma_{MCC} = 0.4$. One sees that the point at which the behavior of the curves changes depends both on σ_{MCC} and n . From Figs 4a and 4b, it is evident that the approximate method for computing P_F slightly overestimates the false alarm probability when compared to the numerical method (see Table V for all values of M and n). Hence, to avoid calculating multiple integrals in (37) and (39), the proposed

approximate method may be efficiently used to address the design problem in (16).

The presented results in recent figures may be used to solve the optimization problem of (16). For example, Figs 3b and 4a reveal that the optimized number of SNMs per unit size is $M = 7$ for $\sigma_{MCC} = 0.1$, when NCCs are spatially correlated and temporary independent for $\xi = 1 - 10^{-6}$, $\gamma = 10^{-5}$, $\sigma_{MCC} = 0.1$ and $n = 9$. Figs 3d and 4b indicate that in the same setting and temporary and spatially correlated NCCs with $\sigma_{MCC} = 0.4$, we need to select $M = 23$. Furthermore, Fig. 3b demonstrates a smaller P_M when SNM observations are spatially independent as opposed to when they are correlated. Hence, if we consider the correlated observations as independent observations in the analyses instead, we will underestimate the required number of SNMs, M . For example, in the same setting with $P_F = 10^{-5}$ to achieve $P_M = 10^{-6}$ we find $M = 10$ for spatially independent SNM observations. However, in the correlated scenario, we need at least $M = 13$.

Figs 5a and 5b show P_M and P_F for NADS in terms of M , for different values of P_F^{NCC} for spatially and temporary correlated NCCs. In Fig. 5b, the results demonstrate that P_F increases with P_F^{NCC} and M . The typical trade-off of false alarm and detection performance of SNM over the NCC is visible in Fig. 5c. Interestingly, P_F^{NCC} affects the overall detection performance of NADS in the same way (Fig. 5a), as it directly influences the NCC detection performance P_M^{NCC} (Fig. 5c). These figures also demonstrate the effect of networking of the SNMs on the performance. Consider the performance of a single SNM in Fig. 5c at $P_F^{NCC} = 10^{-6}$ and $P_M^{NCC} \approx 0.35$. According to results in 5a and 5b, utilizing 20 SNMs leads to significantly improved P_M of 10^{-6} and $P_F \approx 10^{-5}$.

Our experiments (not reported here) reveal that the probability of miss-detection over the NCC noticeably reduces as parameter k increases (this parameter may be used to indicate the disease progress level). Such a behavior then reflects in the overall system performance as depicted in Fig. 5d. One sees that as k increases, P_M reduces much faster with M . The results indicate that if the competitor cell affects the molecular environment more strongly, the proposed NADS detects its presence more easily. A larger value of k in (21), may be interpreted as a disease which has progressed further and hence has altered the status of the molecular environment more significantly from a healthy setting.

The setting of this paper in the special case of spatial and temporal independent noise of SNMs reduces to that of our earlier study in [21]. However, the presented analysis in this work is exact in the said setting, whereas the prior work relies on certain approximations. Specifically, our extensive numerical

TABLE IV: Parameters of numerical results for Figs 2-5d, X:Y:Z denotes the range of parameter as [X,Z] with step size Y, $G = 1$, $NH = 1$, $vol = 1000[nm^3]$.

Parameter	σ_{MCC}	η_1	n	k
Figs 3a-3c	0.1	10^{-6}	1:2:9	2
Figs 3d and 4b	0.4	10^{-6}	1:2:9	2
Fig. 4a	0.1, 0.2:0.2:1	10^{-6}	9	2
Figs 5a- 5c	0.1	$[10^{-6}10^{-5}10^{-4}10^{-3}10^{-2}10^{-1}]$	9	2
Fig. 5d	0.1	0.1	1	1.75:0.5:3.25

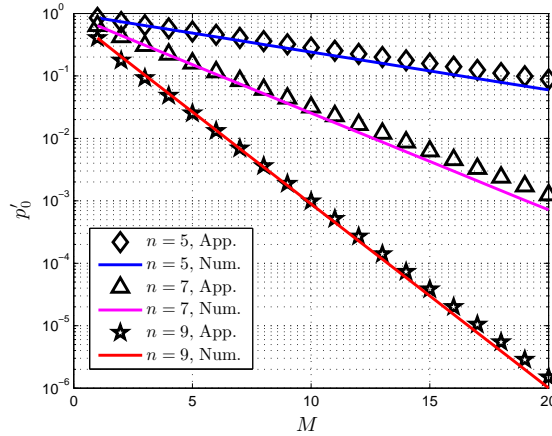


Fig. 2: The probability of receiving no microscale messages at DGN over the spatially and temporally correlated noise of SNMs in presence of abnormality (Solid lines: p'_0 in (45)) and approximation of p'_0 (Markers: \tilde{p}'_0 in (56)), in terms of M for different values of n with $\rho = 0.1$.

results show that the approximated analyses of PF and PM in [21] are respectively a good approximation and an upper bound for the exact values presented here.

VI. CONCLUSIONS

An abnormality detection scheme for detection of competitor cells in a bio-molecular nano-network was proposed. This is motivated for the early detection and classification of diseases and enabling their timely

TABLE V: Numerical results presentation specification for Figs 3-5

Method	Type of Curve	Spatially correlated	Q_D, Q_F	p'_i, p''_i	P_M, P_F
Numerical (Num.)	Solid lines	✓	Numerically computed by (37) and (39)	Approximated by p'_i and p''_i in (56) and (57)	(47) and (48)
Approximated (App.)	Markers only	✓	Approximated by \tilde{Q}_D and \tilde{Q}_F (59) and (60)	Approximated by p'_i and p''_i in (56) and (57)	(47) and (48)
Exact formula spatially independent scenario (Sp. Ind.)	Dashed-dotted lines	×	(40) and (41)	(51) and (52)	(49) and (50)

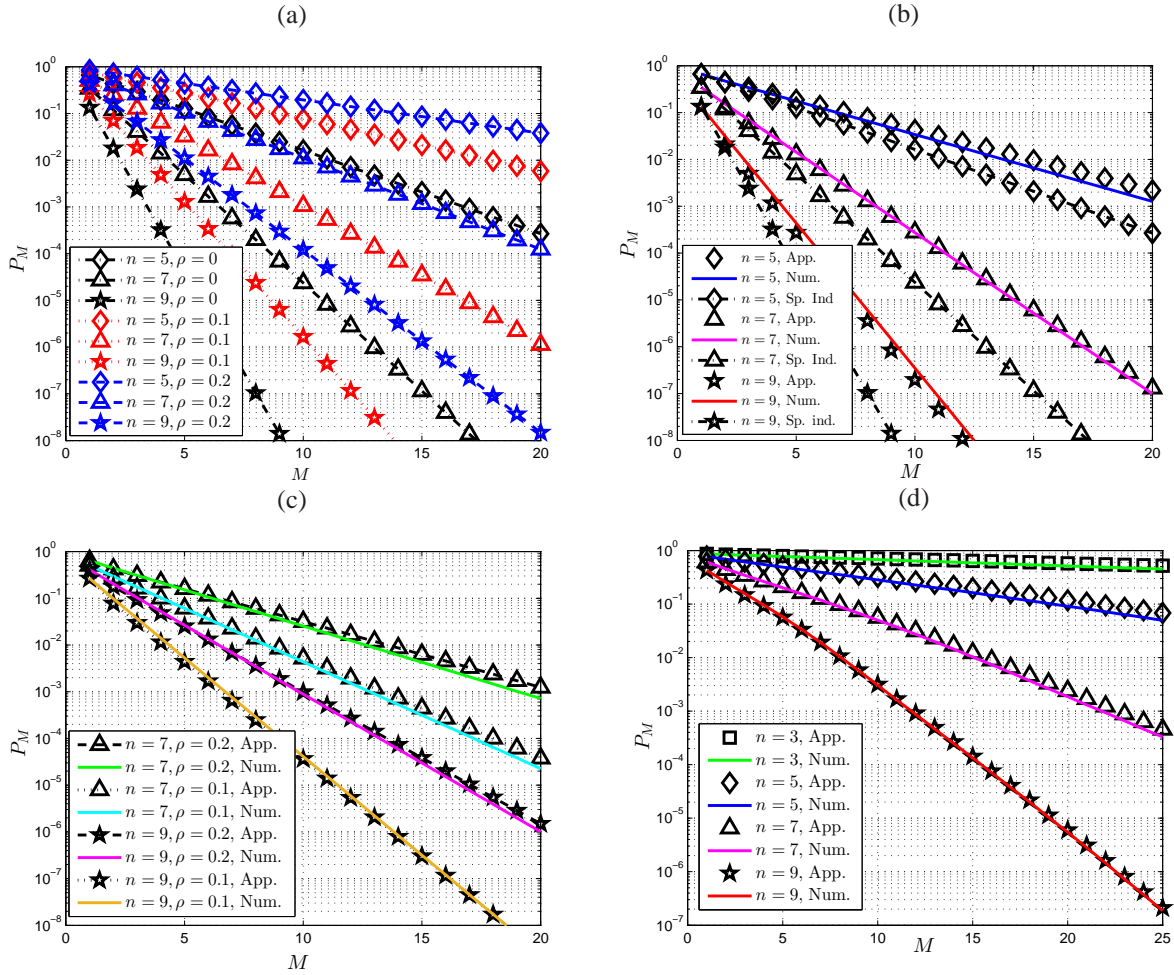


Fig. 3: (a) P_M vs. M for different values of n and ρ in spatially independent and temporally correlated scenario (dashed-dotted $\rho=0$, dotted lines $\rho=0.1$, dashed lines $\rho=0.2$) and $\sigma_{MCC}=0.1$. (b) P_M vs. M for different values of n in spatially independent/correlated and temporally independent scenario, $\rho=0$ and $\sigma_{MCC}=0.1$. (c) P_M vs. M for different values of n and ρ in spatially and temporally correlated scenario. (Dotted lines $\rho=0.1$, dashed lines $\rho=0.2$) and $\sigma_{MCC}=0.1$. (d) P_M in terms of M for different values of n in spatially and temporally correlated scenario, for $\rho=0.2$ and $\sigma_{MCC}=0.4$.

and effective treatment. The proposed NADS is a two-tier network. The sensor nano-machines at the first tier act as receivers of a nano-communications channel modeling the molecular environment. The SNMs then communicate over a noisy channel to a data gathering node, which operates based on an OR fusion rule. The average number of received molecules serves as a feature for detecting the abnormalities at the SNMs. The detection performance of each SNM in presence of Gaussian observation noise was analyzed using a generalized likelihood ratio test. Moreover, the effects of temporal and spatial correlations of the SNMs observations on the detection performance were studied. The reported experiments results reveal that otherwise ignoring possibly existing temporal or spatial correlations would lead to noticeably

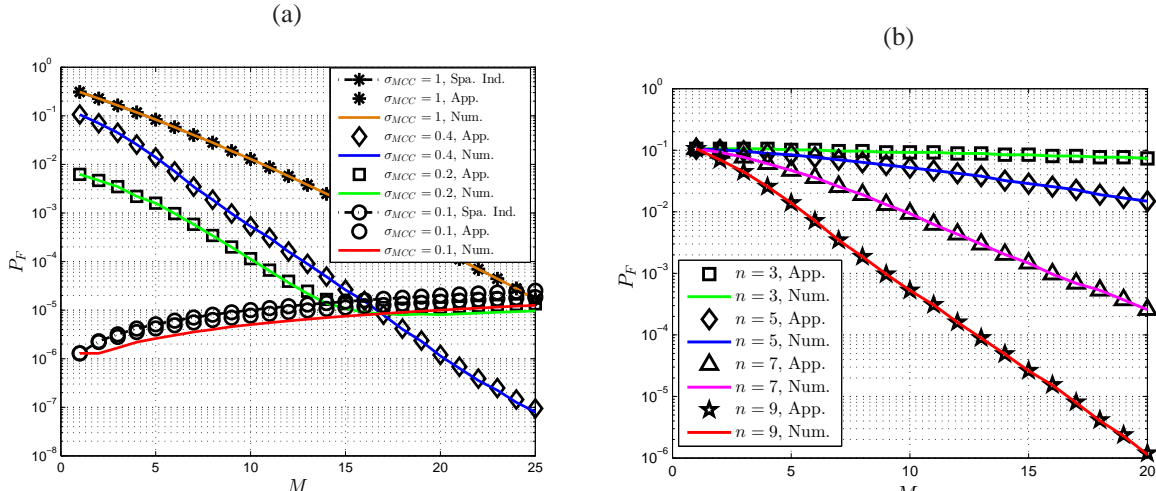


Fig. 4: (a) P_F in terms of M for different values of σ_{MCC} , in spatially correlated/independent and temporary correlated scenario with $\rho = 0.2$. (b) P_F in terms of M for different values of n in spatially and temporally correlated scenario, for $\rho = 0.2$ and $\sigma_{MCC} = 0.4$.

inaccurate performance results. Next, quantifying the overall NADS detection performance, a design problem was set up that quantifies the minimum required concentration of SNMs for a desired level of NADS reliability. The solution determines the optimized operation of detectors for each of the NADS tiers. This in turn facilitates optimized abnormality detection with smallest possible side effects due to the injection of nano-sensors. The results indicate how effective fusion of the noisy observations collected from a number of sensor nano-machines with limited capabilities could provide an acceptable detection performance.

At the current stage of research on detection of diseases at the nano-scale, there are still many interesting open research problems. Here, we state a few of them. In this paper, the detection feature is set based on a mathematical modeling and certain valid approximations. Developing more precise models or obtaining the exact detection feature based on experimental measurements in the target tissue is an interesting research avenue. The side effects of injected SNMs on the molecular environment play an important role in the accuracy of the model and the performance of NADS. Hence, studying those effects is another key aspect of research in this field. Designing practical SNMs for detection of cancer or other diseases and taking the experimental constraints of those SNMs into consideration within the proposed NADS framework poses a number of other interesting and important research problems. Medical imaging is one approach to detection over the MCC; other approaches includes ultrasonic or terahertz communications. Realistic modeling of MCC noise is an interesting issue for enhancing the NADS performance for abnormality detection in a biomolecular environment.

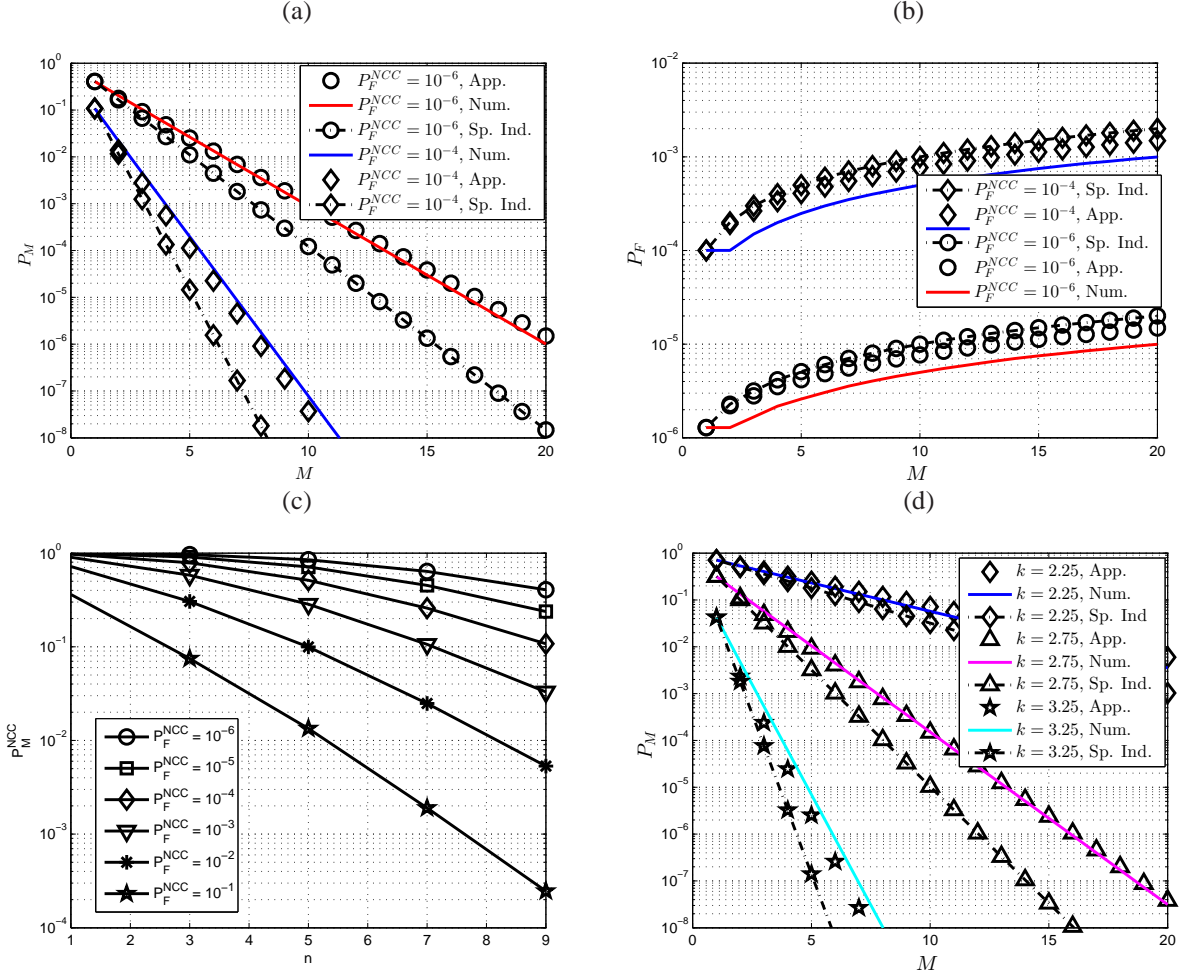


Fig. 5: (a) P_M in terms of M for different values of P_F^{NCC} . (b) P_F in terms of M for different values of P_F^{NCC} all for $\rho = 0.2$ and $\sigma_{MCC} = 0.1$. (c) P_M^{NCC} in terms of n for different values of P_F^{NCC} , $\rho = 0.2$. (d) P_M in terms of M for different values of k , $\rho = 0.2$ and $\sigma_{MCC} = 0.1$.

VII. APPENDICES

A. Proof of Theorem 1

The GLRT [73] for hypothesis test of (17) is given by

$$\frac{\max_{NR \neq NH} P(\mathbf{y}_j^n | NR)}{P(\mathbf{y}_j^n | NH)} = \frac{P(\mathbf{y}_j^n | \widehat{NR}_j)}{P(\mathbf{y}_j^n | NH)} = \frac{\frac{1}{(2\pi)^n / 2 \sigma_{NCC}^n |\Omega^T|^{1/2}} \exp\left(-\frac{1}{2\sigma_{NCC}^2} (\mathbf{y}_j^n - \widehat{NR}^n)^\dagger \Omega^{T-1} (\mathbf{y}_j^n - \widehat{NR}^n)\right)}{\frac{1}{(2\pi)^n / 2 \sigma_{NCC}^n |\Omega^T|^{1/2}} \exp\left(-\frac{1}{2\sigma_{NCC}^2} (\mathbf{y}_j^n - \mathbf{NH}^n)^\dagger \Omega^{T-1} (\mathbf{y}_j^n - \mathbf{NH}^n)\right)} > \tau, \quad (61)$$

where $\widehat{\mathbf{NR}}^n = [\widehat{NR}_j]_{1 \times n}$, $\mathbf{NH}^n = [NH]_{1 \times n}$ and \widehat{NR}_j is given by (26). Simplifying (61) we have

$$\exp \left\{ \frac{-1}{2\sigma_{NCC}^2} \left[\sum_{l=1}^n \sum_{i=1}^n (y_{lj} - \widehat{NR}_j) (y_{ij} - \widehat{NR}_j) \psi_{il}^{TC} - \sum_{l=1}^n \sum_{i=1}^n (y_{lj} - NH) (y_{ij} - NH) \psi_{il}^{TC} \right] \right\} > \tau. \quad (62)$$

Computing the natural Logarithm of (62), we obtain

$$\begin{aligned} & \frac{-1}{2\sigma_{NCC}^2} \left\{ \sum_{l=1}^n \sum_{i=1}^n (y_{lj} - \widehat{NR}_j) (y_{ij} - \widehat{NR}_j) \psi_{il}^{TC} - \right. \\ & \left. \sum_{l=1}^n \sum_{i=1}^n \left((y_{lj} - \widehat{NR}_j) + (\widehat{NR}_j - NH) \right) \left((y_{ij} - \widehat{NR}_j) + (\widehat{NR}_j - NH) \right) \psi_{il}^{TC} \right\} > \log \tau. \end{aligned} \quad (63)$$

Following some manipulations, we have

$$\begin{aligned} & \frac{-1}{2\sigma_{NCC}^2} \left\{ - \sum_{l=1}^n \sum_{i=1}^n (y_{lj} - \widehat{NR}_j) (\widehat{NR}_j - NH) \psi_{il}^{TC} - \right. \\ & \left. \sum_{l=1}^n \sum_{i=1}^n (y_{ij} - \widehat{NR}_j) (\widehat{NR}_j - NH) \psi_{il}^{TC} - \sum_{l=1}^n \sum_{i=1}^n (\widehat{NR}_j - NH)^2 \psi_{il}^{TC} \right\} > \log \tau. \end{aligned} \quad (64)$$

Replacing \widehat{NR}_j from (26) in the first and second terms of RHS of (64), we have

$$\frac{-1}{2\sigma_{NCC}^2} \left[- \sum_{l=1}^n \sum_{i=1}^n (\widehat{NR}_j - NH)^2 \psi_{il}^{TC} \right] > \log \tau \Rightarrow (\widehat{NR}_j - NH)^2 > \frac{2\sigma_{NCC}^2 \log \tau}{\sum_{l=1}^n \sum_{i=1}^n \psi_{il}^{TC}}. \quad (65)$$

With more simplification, the decision region for hypothesis test of (17) is obtained as

$$\begin{cases} H_0 & NH - \tau' < \widehat{NR}_j < NH + \tau' \\ H_1 & \widehat{NR}_j > NH + \tau' \\ & \widehat{NR}_j < NH - \tau', \end{cases} \quad (66)$$

where

$$\tau' \triangleq \sqrt{2\sigma_{NCC}^2 \log(\tau) / \sum_{l=1}^n \sum_{i=1}^n \psi_{il}^{TC}}. \quad (67)$$

For deriving the false-alarm probability of a decision rule, we need to calculate the PDF of \widehat{NR}_j given in (26). The random variables y_{ij} are jointly Gaussian, hence their weighted summation is also Gaussian.

When H_0 is true, the mean of decision variable at the SNM, \widehat{NR}_j is NH and its variance is given by [75]

$$\sigma_D^2 = \left(\sum_{l=1}^n \sum_{i=1}^n \psi_{il}^{TC} \right)^{-2} \left\{ \sum_{l=1}^n \text{var}(\lambda_l) + 2 \sum_{q < l} \text{cov}(\lambda_q, \lambda_l) \right\}. \quad (68)$$

in which $\lambda_l = y_{lj} \sum_{i=1}^n \psi_{il}^{TC}$, the subscript of j in λ_l is dropped due to homogeneous assumption of NCCs for each SNM, $\text{var}(\lambda_l) = \left(\sum_{i=1}^n \psi_{il}^{TC} \right)^2 \sigma_{NCC}^2$, and $\text{cov}(\lambda_q, \lambda_l) = \left(\sum_{i=1}^n \psi_{il}^{TC} \right) \left(\sum_{i=1}^n \psi_{il}^{TC} \right) \omega_{ql}^{TC} \sigma_{NCC}^2$.

We have

$$\sigma_D^2 = \left(\sum_{l=1}^n \sum_{i=1}^n \psi_{il}^{TC} \right)^{-2} \left\{ \sum_{l=1}^n \left(\sum_{i=1}^n \psi_{il}^{TC} \right)^2 \left(\sigma_{NCC}^2 + 2 \sum_{l=1}^{n-1} \sum_{q=l+1}^n \omega_{ql}^{TC} \sigma_{NCC}^2 \right) \right\}. \quad (69)$$

Therefore, the false alarm probability can be expressed by

$$P_F^{NCC} = 1 - \Pr \{ NH - \tau' < \mathcal{N}(NH, \sigma_D^2) < NH + \tau' \mid H_0 \}, \quad (70)$$

and as we desire to have $P_F^{NCC} \leq \eta_1$, we obtain

$$2\phi(\tau'/\sigma_D) - 1 \geq 1 - \eta_1, \quad (71)$$

that is satisfied with equality, when we have

$$\tau' = \sigma_D \phi^{-1} \left(1 - \frac{\eta_1}{2} \right). \quad (72)$$

According to the region of H_1 in (66), P_D^{NCC} can be written as

$$P_D^{NCC} = \Pr \left\{ \widehat{NR}_j < NH - \tau', \widehat{NR}_j > NH + \tau' \mid H_1 \right\}, \quad (73)$$

and due to the Gaussian distribution of \widehat{NR}_j , we have

$$\begin{aligned} P_D^{NCC} &= \Pr \{ \mathcal{N}(NR, \sigma_D^2) < NH - \tau', \mathcal{N}(NR, \sigma_D^2) > NH + \tau' \} = \\ &= 1 - \mathcal{Q} \left(\frac{NH - \tau' - NR}{\sigma_D} \right) + \mathcal{Q} \left(\frac{NH + \tau' - NR}{\sigma_D} \right). \end{aligned} \quad (74)$$

The relation of P_D and NR is evident in (74). When a competitor cell is present in the NCC environment, NR deviates from the NH . For a specific type of competitor cell, considering (21) in (74), P_D^{NCC} can be obtained as

$$\begin{aligned} P_D^{NCC} &= 1 - \mathcal{Q}((NH - \tau' - (1 \pm k\sigma_{NCC}) NH)/\sigma_D) + \mathcal{Q}((NH + \tau' - (1 \pm k\sigma_{NCC}) NH)/\sigma_D) \\ &= 1 - \mathcal{Q}((- \tau' \mp k\sigma_{NCC} NH)/(\sigma_D)) + \mathcal{Q}((\tau' \mp k\sigma_{NCC} NH)/(\sigma_D)). \end{aligned} \quad (75)$$

Replacing τ' from (72) in (75), the following result is obtained

$$P_D^{NCC} = 1 - \mathcal{Q} \left((-\sigma_D \phi^{-1} (1 - \frac{\eta_1}{2}) \mp k \sigma_{NCC} NH) / \sigma_D \right) + \mathcal{Q} \left((\sigma_D \phi^{-1} (1 - \frac{\eta_1}{2}) \mp k \sigma_{NCC} NH) / \sigma_D \right). \quad (76)$$

B. Proof of Lemma 1

It is evident in (26) that \widehat{NR}_j is a weighted sum of y_{ij} 's, which are jointly Gaussian distributed and hence their summation is Gaussian with mean NR . The correlation coefficient of \widehat{NR}_j and \widehat{NR}_q is given by

$$\text{cor}(\widehat{NR}_j, \widehat{NR}_q) = \frac{E \left[\left(\widehat{NR}_j - NR \right) \left(\widehat{NR}_q - NR \right) \right]}{\sqrt{E \left[\left(\widehat{NR}_j - NR \right)^2 \right] E \left[\left(\widehat{NR}_q - NR \right)^2 \right]}}. \quad (77)$$

Using (26), we obtain

$$\text{cor}(\widehat{NR}_j, \widehat{NR}_q) = \frac{E \left[\left(\sum_{l=1}^n \sum_{i=1}^n y_{lj} \psi_{il}^{TC} / \sum_{l=1}^n \sum_{i=1}^n \psi_{il}^{TC} - NR \right) \left(\sum_{l=1}^n \sum_{i=1}^n y_{lq} \psi_{il}^{TC} / \sum_{l=1}^n \sum_{i=1}^n \psi_{il}^{TC} - NR \right) \right]}{\sqrt{E \left[\left(\sum_{l=1}^n \sum_{i=1}^n y_{lj} \psi_{il}^{TC} / \sum_{l=1}^n \sum_{i=1}^n \psi_{il}^{TC} - NR \right)^2 \right] E \left[\left(\sum_{l=1}^n \sum_{i=1}^n y_{lq} \psi_{il}^{TC} / \sum_{l=1}^n \sum_{i=1}^n \psi_{il}^{TC} - NR \right)^2 \right]}}, \quad (78)$$

and following some mathematical manipulation, we have

$$\text{cor}(\widehat{NR}_j, \widehat{NR}_q) = \frac{E \left[\left(\sum_{l=1}^n \sum_{i=1}^n (y_{lj} - NR) \psi_{il}^{TC} \right) \left(\sum_{l=1}^n \sum_{i=1}^n (y_{lq} - NR) \psi_{il}^{TC} \right) \right]}{\sqrt{E \left[\left(\sum_{l=1}^n \sum_{i=1}^n (y_{lj} - NR) \psi_{il}^{TC} \right)^2 \right] E \left[\left(\sum_{l=1}^n \sum_{i=1}^n (y_{lq} - NR) \psi_{il}^{TC} \right)^2 \right]}}. \quad (79)$$

Using the assumption of separability of spatial and temporal correlation as discussed in Section II and some mathematical manipulations, we have

$$\text{cor}(\widehat{NR}_j, \widehat{NR}_q) = \frac{\omega_{jq}^{SC} \left(\sum_{l=1}^n \left(\sigma_{NCC}^2 \left(\sum_{i=1}^n \psi_{il}^{TC} \sum_{i=1}^n \psi_{il}^{TC} \right) + 2 \sum_{k=l+1}^n \omega_{kl}^{TC} \sigma_{NCC}^2 \sum_{i=1}^n \psi_{il}^{TC} \sum_{i=1}^n \psi_{il}^{TC} \right) \right)}{\sum_{l=1}^n \left\{ \left(\sum_{i=1}^n \psi_{il}^{TC} \right)^2 \sigma_{NCC}^2 + 2 \sum_{k=l+1}^n \left(\sum_{i=1}^n \psi_{il}^{TC} \sum_{i=1}^n \psi_{il}^{TC} \right) \omega_{kl}^{TC} \sigma_{NCC}^2 \right\}} = \omega_{jq}^{SC}. \quad (80)$$

C. Proof of Theorem 2

The MAP rule is written as

$$\begin{aligned} & \max_{i \in \{0,1\}} P(H_i|V) \stackrel{(a)}{=} P(H_i|V, W_0) P(W_0|V) + P(H_i|V, W_1) P(W_1|V) \\ & \stackrel{(b)}{=} \max_{i \in \{0,1\}} P(H_i|W_0) P(W_0|V) + P(H_i|W_1) P(W_1|V) \\ & \stackrel{(c)}{=} \max_{i \in \{0,1\}} \frac{P(W_0|H_i)P(H_i)}{P(W_0)} P(W_0|V) + \frac{P(W_1|H_i)P(H_i)}{P(W_1)} P(W_1|V) \end{aligned} \quad (81)$$

where in the probability function of $P(\bullet)$ event of $V = v$ is denoted by V for brevity and events of W_0/W_1 are defined as

$$\begin{cases} W_0 : \sum_{j=1}^M X_j < G \\ W_1 : \sum_{j=1}^M X_j \geq G. \end{cases} \quad (82)$$

In (81), (a) follows from the law of total probability, (b) from Markov property of $H_i \rightarrow W_i \rightarrow V$ and (c) follows from the Bayes rule. Simplifying (81), we have

$$\begin{aligned} & \frac{P(W_0|H_0)P(H_0)}{P(W_0)} P(W_0|V) + \frac{P(W_1|H_0)P(H_0)}{P(W_1)} P(W_1|V) \stackrel{H_0}{>} \\ & \frac{P(W_0|H_1)P(H_1)}{P(W_0)} P(W_0|V) + \frac{P(W_1|H_1)P(H_1)}{P(W_1)} P(W_1|V) \stackrel{(a)}{\Rightarrow} \\ & \frac{(1-Q_F)P(H_0)}{P(W_0)} P(W_0|V) + \frac{Q_F P(H_0)}{1-P(W_0)} P(W_1|V) \stackrel{H_0}{>} \frac{(1-Q_D)P(H_1)}{P(W_0)} P(W_0|V) + \frac{Q_D P(H_1)}{1-P(W_0)} P(W_1|V) \stackrel{(b)}{\Rightarrow} \\ & \frac{(1-Q_F)P(H_0)}{P(W_0)} \frac{P(V|W_0)P(W_0)}{P(V)} + \frac{Q_F P(H_0)}{1-P(W_0)} \frac{P(V|W_1)P(W_1)}{P(V)} \stackrel{H_0}{>} \\ & \frac{(1-Q_D)P(H_1)}{P(W_0)} \frac{P(V|W_0)P(W_0)}{P(V)} + \frac{Q_D P(H_1)}{1-P(W_0)} \frac{P(V|W_1)P(W_1)}{P(V)} \Rightarrow \\ & (1-Q_F)P(H_0)P(V|W_0) + Q_F P(H_0)P(V|W_1) \stackrel{H_0}{>} (1-Q_D)P(H_1)P(V|W_0) + Q_D P(H_1)P(V|W_1) \end{aligned} \quad (83)$$

where, (a) is derived based on definition of Q_F and Q_D respectively in (36) and (38), (b) is derived based on the Bayes rule. In (83), $P(V|W_0)$ and $P(V|W_1)$ are given by

$$\begin{aligned} P(V|W_0) &= \frac{1}{\sqrt{2\pi\sigma_{MCC}^2}} \exp\left(\frac{-V^2}{2\sigma_{MCC}^2}\right) \quad (84) \\ P(V|W_1) &= P\left(V \left| \sum_{j=1}^M X_j \geq G\right.\right) = P\left(V \left| \sum_{j=1}^M X_j = G \cup \dots \cup \sum_{j=1}^M X_j = MG\right.\right) \\ & \stackrel{(a)}{=} \frac{P\left(\sum_{j=1}^M X_j = G \cup \dots \cup \sum_{j=1}^M X_j = MG \mid V\right) P(V)}{P\left(\sum_{j=1}^M X_j = G \cup \dots \cup \sum_{j=1}^M X_j = MG\right)} \stackrel{(b)}{=} \frac{P\left(\sum_{j=1}^M X_j = G \cup \dots \cup \sum_{j=1}^M X_j = MG \mid V\right) P(V)}{1 - P\left(\sum_{j=1}^M X_j = 0\right)} \\ & = \frac{P\left(\left\{\sum_{j=1}^M X_j = G \cup \dots \cup \sum_{j=1}^M X_j = MG\right\} \cap V\right)}{1 - P\left(\sum_{j=1}^M X_j = 0\right)} \stackrel{(c)}{=} \frac{P\left(\left(\left\{\sum_{j=1}^M X_j = G\right\} \cap V\right) \cup \dots \cup \left(\left\{\sum_{j=1}^M X_j = MG\right\} \cap V\right)\right)}{1 - P\left(\sum_{j=1}^M X_j = 0\right)} \\ & \stackrel{(d)}{=} \frac{\sum_{l=1}^M P\left(\left\{\sum_{j=1}^M X_j = lG\right\} \cap V\right)}{1 - P\left(\sum_{j=1}^M X_j = 0\right)} = \frac{\sum_{l=1}^M P\left(V \left| \sum_{j=1}^M X_j = lG\right.\right) P\left(\sum_{j=1}^M X_j = lG\right)}{1 - P\left(\sum_{j=1}^M X_j = 0\right)} \\ & \stackrel{(e)}{=} \frac{1}{(1-p_0)\sqrt{2\pi\sigma_{MCC}^2}} \sum_{l=1}^M p_l \exp\left(\frac{-(V-lG)^2}{2\sigma_{MCC}^2}\right). \end{aligned} \quad (85)$$

Here, (a) follows from the Bayes rule, (b) follows from definition of event of X_j , (c) follows from De Morgans law, (d) follows since the events $X_j = lG, \forall l$ are mutually exclusive, and (e) follows since the noise of MCC is Gaussian. Hence, replacing (84) and (85) in (83) we have

$$\begin{aligned}
& (1 - Q_F) P(H_0) \frac{1}{\sqrt{2\pi\sigma_{MCC}^2}} \exp\left(\frac{-V^2}{2\sigma_{MCC}^2}\right) + Q_F P(H_0) \frac{1}{(1-p_0)\sqrt{2\pi\sigma_{MCC}^2}} \sum_{l=1}^M p_l \exp\left(\frac{-(V-lG)^2}{2\sigma_{MCC}^2}\right) \stackrel{H_0}{>} \\
& (1 - Q_D) P(H_1) \frac{1}{\sqrt{2\pi\sigma_{MCC}^2}} \exp\left(\frac{-V^2}{2\sigma_{MCC}^2}\right) + Q_D P(H_1) \frac{1}{(1-p_0)\sqrt{2\pi\sigma_{MCC}^2}} \sum_{l=1}^M p_l \exp\left(\frac{-(V-lG)^2}{2\sigma_{MCC}^2}\right), \stackrel{H_0}{>}
\end{aligned} \tag{86}$$

which simplifies to

$$\begin{aligned}
& ((1 - Q_F) P(H_0) - (1 - Q_D) P(H_1)) \exp\left(\frac{-V^2}{2\sigma_{MCC}^2}\right) + \\
& (Q_F P(H_0) - Q_D P(H_1)) \frac{1}{(1-p_0)} \sum_{l=1}^M p_l \exp\left(\frac{-(V-lG)^2}{2\sigma_{MCC}^2}\right) \stackrel{H_0}{>} 0.
\end{aligned} \tag{87}$$

The decision region of DGN is then $V \stackrel{H_0}{<} V^{THR}$, where V^{THR} is derived numerically from (87).

D. Appendix D. Proof of Theorem 3

The probability of detection, P_D , is given by

$$\begin{aligned}
P_D &= P(V_{H_1} | H_1) \stackrel{(a)}{=} P(V_{H_1} | H_1, W_0) P(W_0 | H_1) + P(V_{H_1} | H_1, W_1) P(W_1 | H_1) \\
&\stackrel{(b)}{=} P(V_{H_1} | H_1, W_0) (1 - Q_D) + P(V_{H_1} | H_1, W_1) Q_D \\
&\stackrel{(c)}{=} P\left(V_{H_1} | H_1, \sum_{j=1}^M X_j = 0\right) (1 - Q_D) + P\left(V_{H_1} | H_1, \sum_{j=1}^M X_j \geq G\right) Q_D \\
&\stackrel{(d)}{=} P\left(V_{H_1} | H_1, \sum_{j=1}^M X_j = 0\right) (1 - Q_D) + \frac{\sum_{l=1}^M P\left(V_{H_1} | \sum_{j=1}^M X_j = lG, H_1\right) P\left(\sum_{j=1}^M X_j = lG | H_1\right)}{1 - P\left(\sum_{j=1}^M X_j = 0 | H_1\right)} Q_D \\
&= Q\left(\frac{V^{THR}}{\sigma_{MCC}}\right) (1 - Q_D) + \frac{\sum_{l=1}^M Q\left(\frac{V^{THR} - lG}{\sigma_{MCC}}\right) p'_l}{1 - p'_0} Q_D,
\end{aligned} \tag{88}$$

where, V_{H_1} is the event of $V > V^{THR}$, (a) follows from the law of total probability, (b) is derived based on definitions of Q_F and Q_D respectively in (36) and (38), (c) is derived based on definitions of W_0 and W_1 in (82), and $p'_l = \Pr\{U = lG | H_1\}$, $l \in [0, M]$ is given by (45), and (d) is derived as follows,

$$\begin{aligned}
& P\left(V_{H_1} \left| H_1, \sum_{j=1}^M X_j \geq G\right.\right) = P\left(V_{H_1} \left| H_1 \cap \left(\sum_{j=1}^M X_j = G \cup \dots \cup \sum_{j=1}^M X_j = MG\right)\right.\right) \\
&\stackrel{(a)}{=} \frac{P\left(\left(\sum_{j=1}^M X_j = G \cup \dots \cup \sum_{j=1}^M X_j = MG\right) \cap H_1 \left| V_{H_1}\right.\right) P(V_{H_1})}{P\left(\left(\sum_{j=1}^M X_j = G \cup \dots \cup \sum_{j=1}^M X_j = MG\right) \cap H_1\right)} \stackrel{(b)}{=} \frac{P\left(\left(\left\{\sum_{j=1}^M X_j = G\right\} \cap V_{H_1} \cap H_1\right) \cup \dots \cup \left(\left\{\sum_{j=1}^M X_j = MG\right\} \cap V_{H_1} \cap H_1\right)\right)}{P\left(\left(\sum_{j=1}^M X_j = G \cup \dots \cup \sum_{j=1}^M X_j = MG\right) \cap H_1\right)} \\
&\stackrel{(c)}{=} \frac{\sum_{l=1}^M P\left(\left\{\sum_{j=1}^M X_j = lG\right\} \cap V_{H_1} \cap H_1\right)}{P\left(\left(\sum_{j=1}^M X_j = G \cup \dots \cup \sum_{j=1}^M X_j = MG\right) \cap H_1\right)} \stackrel{(d)}{=} \frac{\sum_{l=1}^M P\left(V_{H_1} \left| \sum_{j=1}^M X_j = lG \cap H_1\right.\right) P\left(\sum_{j=1}^M X_j = lG \cap H_1\right)}{P\left(\left(\sum_{j=1}^M X_j = G \cup \dots \cup \sum_{j=1}^M X_j = MG\right) \cap H_1\right)} \\
&\stackrel{(e)}{=} \frac{\sum_{l=1}^M P\left(V_{H_1} \left| \sum_{j=1}^M X_j = lG \cap H_1\right.\right) P\left(\sum_{j=1}^M X_j = lG | H_1\right) P(H_1)}{P\left(\left(\sum_{j=1}^M X_j = G \cup \dots \cup \sum_{j=1}^M X_j = MG\right) | H_1\right) P(H_1)} \stackrel{(f)}{=} \frac{\sum_{l=1}^M P\left(V_{H_1} \left| \sum_{j=1}^M X_j = lG \cap H_1\right.\right) P\left(\sum_{j=1}^M X_j = lG | H_1\right)}{1 - P\left(\sum_{j=1}^M X_j = 0 | H_1\right)}.
\end{aligned} \tag{89}$$

The steps in deriving (89) are similar to those in (85). In a similar way, the NADS probability of false alarm may be computed as

$$\begin{aligned}
P_F &= P(V_{H_0}|H_0) = P(V_{H_0}|H_0, W_0)P(W_0|H_0) + P(V_{H_0}|H_0, W_1)P(W_1|H_0) \\
&= P(V_{H_0}|H_0, W_0)(1 - Q_F) + P(V_{H_0}|H_0, W_1)Q_F \\
&= P\left(V_{H_0}|H_0, \sum_{j=1}^M X_j = 0\right)(1 - Q_F) + P\left(V_{H_0}|H_0, \sum_{j=1}^M X_j \geq G\right)Q_F \\
&= P\left(V_{H_0}|H_0, \sum_{j=1}^M X_j = 0\right)(1 - Q_F) + \frac{\sum_{l=1}^M P\left(V_{H_0} \left| \sum_{j=1}^M X_j = lG, H_0 \right.\right) P\left(\sum_{j=1}^M X_j = lG | H_0\right)}{1 - P\left(\sum_{j=1}^M X_j = 0 | H_0\right)} Q_F \\
&= \mathcal{Q}\left(\frac{V^{THR}}{\sigma_{MCC}}\right)(1 - Q_F) + \frac{\sum_{l=1}^M \mathcal{Q}\left(\frac{V^{THR} - lG}{\sigma_{MCC}}\right) p''_l}{1 - p''_0} Q_F.
\end{aligned} \tag{90}$$

where, V_{H_0} is the event of $V < V^{THR}$, $p''_l = \Pr\{U = lG | H_0\}$, $l \in [1, M]$ is given by (46) and the steps in deriving (90) are similar to those in (88).

E. Proof of Lemma 2

We consider a homogenous molecular environment, if we assume $\widehat{NR}_1 \approx \widehat{NR}_2 \approx \dots \approx \widehat{NR}_M \approx \widehat{NR}$, p'_l in (45) may be approximated as follows

$$\begin{aligned}
p'_l &\approx \binom{M}{l} (2\pi)^{-M/2} \sigma_D^{-M} |\Omega^{SC}|^{-1/2} \int_A \exp\left(-\frac{l}{2M\sigma_D^2} (\widehat{NR} - NR)^2 [\mathbf{1}]^\dagger \Omega^{SC^{-1}} [\mathbf{1}]\right) d\widehat{NR} \\
&\int_{A^C} \exp\left(-\frac{M-l}{2M\sigma_D^2} (\widehat{NR} - NR)^2 [\mathbf{1}]^\dagger \Omega^{SC^{-1}} [\mathbf{1}]\right) d\widehat{NR},
\end{aligned} \tag{91}$$

where, $[\mathbf{1}] = [1, \dots, 1]_{1 \times M}$. Using Holder's inequality [76] in the RHS of above equation, we have

$$\begin{aligned}
&\int_A \exp\left(-\frac{l}{2M\sigma_D^2} (\widehat{NR} - NR)^2 [\mathbf{1}]^\dagger \Omega^{SC^{-1}} [\mathbf{1}]\right) d\widehat{NR} \times \\
&\int_{A^C} \exp\left(-\frac{M-l}{2M\sigma_D^2} (\widehat{NR} - NR)^2 [\mathbf{1}]^\dagger \Omega^{SC^{-1}} [\mathbf{1}]\right) d\widehat{NR} \leq \\
&\left\{ \int_A \exp\left(-\frac{1}{2\sigma_D^2} (\widehat{NR} - NR)^2\right) d\widehat{NR} \right\}^{\frac{l}{M} [\mathbf{1}]^\dagger \Omega^{SC^{-1}} [\mathbf{1}]} \times \\
&\left\{ \int_{A^C} \exp\left(-\frac{1}{2\sigma_D^2} (\widehat{NR} - NR)^2\right) d\widehat{NR} \right\}^{\frac{M-l}{M} [\mathbf{1}]^\dagger \Omega^{SC^{-1}} [\mathbf{1}]} = \\
&\left(\sqrt{2\pi\sigma_D^2}\right)^{[\mathbf{1}]^\dagger \Omega^{SC^{-1}} [\mathbf{1}]^T} \left\{ \int_A \frac{1}{(\sqrt{2\pi\sigma_D})} \exp\left(-\frac{1}{2\sigma_D^2} (\widehat{NR} - NR)^2\right) d\widehat{NR} \right\}^{\frac{l}{M} [\mathbf{1}]^\dagger \Omega^{SC^{-1}} [\mathbf{1}]} \times \\
&\left\{ \int_{A^C} \frac{1}{(\sqrt{2\pi\sigma_D})} \exp\left(-\frac{1}{2\sigma_D^2} (\widehat{NR} - NR)^2\right) d\widehat{NR} \right\}^{\frac{M-l}{M} [\mathbf{1}]^\dagger \Omega^{SC^{-1}} [\mathbf{1}]} .
\end{aligned} \tag{92}$$

Considering only the first component in Taylor expansion of the first term in RHS of the above inequality

$$p'_l \approx \binom{M}{l} (1 - P_D^{NCC})^{\frac{M-l}{M} ([\mathbf{1}]^\dagger \Omega^{SC^{-1}} [\mathbf{1}])} (P_D^{NCC})^{\frac{l}{M} ([\mathbf{1}]^\dagger \Omega^{SC^{-1}} [\mathbf{1}])}. \tag{93}$$

The RHS of (93) is denoted by \tilde{p}'_l and serves as an efficient approximation of p'_l . The fitting parameter α is obtained numerically for best approximation (See Section V). In a similar manner \tilde{p}''_l in (46) may be calculated. In (58) \tilde{p}_l may be calculated simply by replacing p'_l and p''_l with \tilde{p}'_l and \tilde{p}''_l in (44).

REFERENCES

- [1] A. Jemal, F. Bray, and et al., “Global cancer statistics,” *CA: A Cancer Journal for Clinicians*, vol. 61, no. 2, pp. 69–90, 2011.
- [2] R. John and H. Ros, “The global economic of cancer report,” The American society of cancer, Tech. Rep., Feb. 2000.
- [3] P. Qiu, J. Wang, and K. Liu, “Genomic processing for cancer classification and prediction - abroad review of the recent advances in model-based genomic and proteomic signal processing for cancer detection,” *IEEE Signal Proc. Mag.*, vol. 24, no. 1, pp. 100–110, Jan 2007.
- [4] —, “Cancer nanotechnology: opportunities and challenges,” *Nat Rev Cancer*, vol. 5, no. 1, pp. 161–171, Mar 2005.
- [5] M. M.-C. Cheng, G. Cuda, and et al., “Nanotechnologies for biomolecular detection and medical diagnostics,” *Current Opinion in Chemical Biology*, vol. 10, no. 1, pp. 11 – 19, 2006.
- [6] J. C. Chang, E. C. Wooten, and et al., “Gene expression profiling for the prediction of therapeutic response to docetaxel in patients with breast cancer,” *The Lancet*, vol. 362, no. 9381, pp. 362 – 369, 2003.
- [7] L. J. van ’t Veer and et al., “Gene expression profiling predicts clinical outcome of breast cancer,” *Nature*, vol. 415, no. 6871, pp. 530–536, 2002.
- [8] E. Stern, A. Vacic, and et al., “Label-free biomarker detection from whole blood,” *Nat Nano*, vol. 5, no. 2, pp. 138–142, 2010.
- [9] G. Peng, M. Hakim, and et al., “Detection of lung, breast, colorectal, and prostate cancers from exhaled breath using a single array of nanosensors,” *Br J Cancer*, vol. 103, no. 4, pp. 542–551, 2010.
- [10] M. J. Gunter and et al., “Insulin, insulin-like growth factor-i, and risk of breast cancer in postmenopausal women,” *Journal of the National Cancer Institute*, vol. 101, no. 1, pp. 48–60, 2009.
- [11] C. Danelon, M. Lindemann, and et al., “Channel-forming membrane proteins as molecular sensors,” *IEEE Trans.on NanoBioscience*, vol. 3, no. 1, pp. 46–48, March 2004.
- [12] A. SalmanOgli, A. Rostami, and M. Abasi, “Design and simulation of nano-bio sensors for dye molecules targeting to enhance targeting efficiency (smart targeting),” *IEEE Trans. on NanoBioscience*, vol. 12, no. 1, pp. 21–28, March 2013.
- [13] S. Sanga, J. P. Sinek, and et al., “Mathematical modeling of cancer progression and response to chemotherapy,” *Expert Review of Anticancer Therapy*, vol. 6, no. 10, pp. 1361–1376, 2006.
- [14] V. Cristini, J. Lowengrub, and Q. Nie, “Journal of mathematical biology,” *IEEE Signal Proc. Mag.*, vol. 46, no. 3, pp. 191–224, 2003.
- [15] B. Atakan and O. Akan, “An information theoretical approach for molecular communication,” in *2nd Bio-Inspired Models of Network, Information and Computing Systems*, Dec 2007, pp. 33–40.
- [16] —, “On channel capacity and error compensation in molecular communication,” *Trans. on Compu. Sys. Biology X*, vol. 5410, pp. 59–80, 2008.
- [17] M. Pierobon and I. Akyildiz, “Diffusion-based noise analysis for molecular communication in nanonetworks,” *IEEE Trans. on Signal Proc.*, vol. 59, no. 6, pp. 2532–2547, June 2011.
- [18] Y. Savir and T. Tlusty, “Optimal design of a molecular recognizer: Molecular recognition as a bayesian signal detection problem,” *IEEE J. of Selected Topics in Signal Proc.*, vol. 2, no. 3, pp. 390–399, June 2008.
- [19] T. Nakano, T. Suda, and et al., “Molecular communication among biological nanomachines: A layered architecture and research issues,” *IEEE Trans. on NanoBioscience*, vol. 13, no. 3, pp. 169–197, Sept 2014.
- [20] I. Akyildiz and J. Jornet, “The internet of nano-things,” *IEEE Wireless Commun.*, vol. 17, no. 6, pp. 58–63, December 2010.
- [21] S. Ghavami, F. Lahouti, and A. Masoudi-Nejad, “Modeling and analysis of abnormality detection in biomolecular nano-networks,” *Nano Communication Networks*, vol. 3, no. 4, pp. 229 – 241, 2012.
- [22] X. Wu, H. Liu, and et al., “Immunofluorescent labeling of cancer marker her2 and other cellular targets with semiconductor quantum dots,” *Nat Biotech*, vol. 21, no. 1, pp. 41–46, 2003.
- [23] J. K. Jaiswal, H. Mattoussi, and et al., “Long-term multiple color imaging of live cells using quantum dot bioconjugates,” *Nat Biotech*, vol. 21, no. 1, pp. 47–51, 2003.

- [24] X. Huang, X. Peng, and et al., "A reexamination of active and passive tumor targeting by using rod-shaped gold nanocrystals and covalently conjugated peptide ligands," *ACS Nano*, vol. 4, no. 10, pp. 5887–5896, 2010.
- [25] R. Lvy, U. Shaheen, and et al., "Gold nanoparticles delivery in mammalian live cells: a critical review," *Nano Reviews*, vol. 1, no. 0, 2010.
- [26] E. A. Neuwelt, P. Varallyay, and et al., "Imaging of iron oxide nanoparticles by mr and light microscopy in patients with malignant brain tumours," *Neuropathology and Applied Neurobiology*, vol. 30, no. 5, pp. 456–471, 2004.
- [27] F. K. Moritz, M. Umar, and et al., "A multimodal nanoparticle for preoperative magnetic resonance imaging and intraoperative optical brain tumor delineation," *Journal of Cancer Research*, vol. 63, no. 12, pp. 8122 – 8125, 2003.
- [28] M. O. Oyewumi, R. A. Yokel, and et al., "Comparison of cell uptake, biodistribution and tumor retention of folate-coated and peg-coated gadolinium nanoparticles in tumor-bearing mice," *Journal of Controlled Release*, vol. 95, no. 3, pp. 613 – 626, 2004.
- [29] L. Levy, Y. Sahoo, and et al., "Nanochemistry: Synthesis and characterization of multifunctional nanoclinics for biological applications," *Chemistry of Materials*, vol. 14, no. 9, pp. 3715–3721, 2002.
- [30] E. Bergey, L. Levy, and et al., "Dc magnetic field induced magnetocytolysis of cancer cells targeted by lh-rh magnetic nanoparticles in vitro," *Biomedical Microdevices*, vol. 4, no. 4, pp. 293–299, 2002.
- [31] A. Bogdanovm, R. Weissleder, and et al., "Annexin v-clio: a nanoparticle for detecting apoptosis by mri," *Journal of Molecular Imaging*, vol. 1, no. 2, pp. 1536–0121, 2002.
- [32] F. Yan, H. Xu, and et al., "Synthesis and characterization of silica-embedded iron oxide nanoparticles for magnetic resonance imaging," *Journal of Nanoscience and Nanotechnology*, vol. 4, no. 1-2, pp. 72–76, 2004.
- [33] A. P. Alivisatos, "Semiconductor clusters, nanocrystals, and quantum dots," *Science*, vol. 271, no. 5251, pp. 933–937, 1996.
- [34] W. C. Chan, D. J. Maxwell, and et al., "Luminescent quantum dots for multiplexed biological detection and imaging," *Current Opinion in Biotechnology*, vol. 13, no. 1, pp. 40 – 46, 2002.
- [35] A. M. Derfus, W. C. W. Chan, and S. N. Bhatia, "Probing the cytotoxicity of semiconductor quantum dots," *Nano Letters*, vol. 4, no. 1, pp. 11–18, 2004.
- [36] E. B. Voura, J. K. Jaiswal, and et al., "Tracking metastatic tumor cell extravasation with quantum dot nanocrystals and fluorescence emission-scanning microscopy," *Nat Med*, vol. 10, no. 9, pp. 993–998, 2004.
- [37] Y. Cui, Q. Wei, and et al., "Nanowire nanosensors for highly sensitive and selective detection of biological and chemical species," *Science*, vol. 293, no. 5533, pp. 1289–1292, 2001.
- [38] J. R. Heath, "Nanosystems biology and cancer," in *Abstracts of Papers of the American Chemical Society*, vol. 230, Aug 2005, p. U187.
- [39] R. J. Chen, S. Bangsaruntip, and et al., "Noncovalent functionalization of carbon nanotubes for highly specific electronic biosensors," *Proceedings of the National Academy of Sciences*, vol. 100, no. 9, pp. 4984–4989, 2003.
- [40] A. T. Woolley, C. Guillemette, and et al., "Direct haplotyping of kilobase-size dna using carbon nanotube probes," *Nat Biotech*, vol. 18, no. 7, pp. 760–763, 2000.
- [41] R. Duncan, "The dawning era of polymer therapeutics," *Nat Rev Drug Discov*, vol. 2, no. 5, pp. 347–360, 2003.
- [42] A. H. Nashat, M. Moronne, and M. Ferrari, "Detection of functional groups and antibodies on microfabricated surfaces by confocal microscopy," *Biotechnology and Bioengineering*, vol. 60, no. 2, pp. 137–146, 1998.
- [43] S. Santra, P. Zhang, and et al., "Conjugation of biomolecules with luminophore-doped silica nanoparticles for photostable biomarkers," *Analytical Chemistry*, vol. 73, no. 20, pp. 4988–4993, 2001.
- [44] X. Zhao, R. Tapeç-Dytioco, and W. Tan, "Ultrasensitive dna detection using highly fluorescent bioconjugated nanoparticles," *Journal of the American Chemical Society*, vol. 125, no. 38, pp. 11 474–11 475, 2003.
- [45] F. Wang, L. Liu, and W. J. Li*, "Graphene-based glucose sensors: A brief review," *IEEE Trans. on NanoBioscience*, vol. 14, no. 8, pp. 818–834, Dec 2015.
- [46] E. Zarepour, N. Hassan, M. Hassan, C. T. Chou, and M. E. Warkiani, "Design and analysis of a wireless nanosensor network for monitoring human lung cells," in *Proceedings of the 10th EAI International Conference on Body Area Networks*, ser. BodyNets '15. ICST, Brussels, Belgium, Belgium: ICST (Institute for Computer Sciences, Social-Informatics and Telecommunications Engineering), 2015, pp. 139–145.
- [47] M. S. Mannoor, H. Tao, J. D. Clayton, A. Sengupta, D. L. Kaplan, R. R. Naik, N. Verma, F. G. Omenetto, and M. C. McAlpine, "Graphene-based wireless bacteria detetction on tooth enamel," *Nature Communications*, vol. 3, pp. 1–8, Mar 2012.

- [48] I. F. Akyildiz, M. Pierobon, S. Balasubramaniam, and Y. Koucheryavy, "The internet of bio-nano things," *IEEE Communications Magazine*, vol. 53, no. 3, pp. 32–40, March 2015.
- [49] I. F. Akyildiz, F. Brunetti, and C. Blzquez, "Nanonetworks: A new communication paradigm," *Computer Networks*, vol. 52, no. 12, pp. 2260 – 2279, 2008.
- [50] G. E. Santagati, T. Melodia, L. Galluccio, and S. Palazzo, "Ultrasonic networking for e-health applications," *IEEE Wireless Commun.*, vol. 20, no. 4, pp. 74–81, August 2013.
- [51] —, "Medium access control and rate adaptation for ultrasonic intrabody sensor networks," *IEEE/ACM Transactions on Networking*, vol. 23, no. 4, pp. 1121–1134, Aug 2015.
- [52] H. Guo, P. Johari, J. M. Jornet, and Z. Sun, "Intra-body optical channel modeling for in vivo wireless nanosensor networks," *IEEE Transactions on NanoBioscience*, vol. 15, no. 1, pp. 41–52, Jan 2016.
- [53] J. M. Jornet and I. F. Akyildiz, "Channel modeling and capacity analysis for electromagnetic wireless nanonetworks in the terahertz band," *IEEE Trans. on Wireless Communications*, vol. 10, no. 10, pp. 3211–3221, October 2011.
- [54] G. Tkacik, A. M. Walczak, and W. Bialek, "Optimizing information flow in small genetic networks. iii. a self-interacting gene," *Phys. Rev. E*, vol. 85, p. 041903, Apr 2012.
- [55] —, "Optimizing information flow in small genetic networks," *Phys. Rev. E*, vol. 80, p. 031920, Sep 2009.
- [56] A. M. Walczak, G. c. v. Tkačik, and W. Bialek, "Optimizing information flow in small genetic networks. ii. feed-forward interactions," *Phys. Rev. E*, vol. 81, p. 041905, Apr 2010.
- [57] F. Tostevin and P. R. ten Wolde, "Mutual information in time-varying biochemical systems," *Phys. Rev. E*, vol. 81, p. 061917, Jun 2010.
- [58] "Ieee recommended practice for nanoscale and molecular communication framework," *IEEE Std 1906.1-2015*, pp. 1–64, Jan 2016.
- [59] V. Krivan, P. Lnsk, and J. P. Rospars, "Coding of periodic pulse stimulation in chemoreceptors," *Biosystems*, vol. 67, no. 13, pp. 121 – 128, 2002.
- [60] M. Saxton, "Anomalous diffusion due to binding: a monte carlo study," *Biophysical Journal*, vol. 70, no. 3, pp. 1250 – 1262, 1996.
- [61] C. J. Camacho, S. Kimura, and et al, "Kinetics of desolvation-mediated proteinprotein binding," *Biophysical Journal*, vol. 78, no. 3, pp. 1094 – 1105, 2000.
- [62] B. Li, M. G. Genton, and M. Sherman, "Testing the covariance structure of multivariate random fields," *Biometrika*, vol. 95, no. 4, pp. 813–829, 2008.
- [63] H. Wackernagel, *Multivariate geostatistics: an introduction with applications*, 2nd ed. Springer-Verlag, 2003.
- [64] M. J. Moore, T. Suda, and K. Oiwa, "Molecular communication: modeling noise effects on information rate," *IEEE Trans. on NanoBioscience*, vol. 8, no. 2, pp. 169–180, June 2009.
- [65] M. Pierobon and I. F. Akyildiz, "Noise analysis in ligand-binding reception for molecular communication in nanonetworks," *IEEE Trans. on Signal Processing*, vol. 59, no. 9, pp. 4168–4182, Sept 2011.
- [66] M. U. Mahfuz, D. Makrakis, and H. T. Mouftah, "A comprehensive study of sampling-based optimum signal detection in concentration-encoded molecular communication," *IEEE Trans. on NanoBioscience*, vol. 13, no. 3, pp. 208–222, Sept 2014.
- [67] —, "Strength-based optimum signal detection in concentration-encoded pulse-transmitted {OOK} molecular communication with stochastic ligand-receptor binding," *Simulation Modelling Practice and Theory*, vol. 42, pp. 189 – 209, 2014.
- [68] S. Ghavami, R. S. Adve, and F. Lahouti, "Information rates of ask-based molecular communication in fluid media," *IEEE Trans. on Molecular, Biological and Multi-Scale Communications*, vol. 1, no. 3, pp. 277–291, Sept 2015.
- [69] M. kr Kuran, H. B. Yilmaz, T. Tugcu, and B. zerman, "Energy model for communication via diffusion in nanonetworks," *Nano Communication Networks*, vol. 1, no. 2, pp. 86 – 95, 2010.
- [70] D. Kilinc and O. B. Akan, "Receiver design for molecular communication," *IEEE Journal on Selected Areas in Communications*, vol. 31, no. 12, pp. 705–714, December 2013.
- [71] A. Noel, K. C. Cheung, and R. Schober, "Improving receiver performance of diffusive molecular communication with enzymes," *IEEE Transactions on NanoBioscience*, vol. 13, no. 1, pp. 31–43, March 2014.
- [72] H. B. Yilmaz, C.-B. Chae, B. Tepekule, and A. E. Pusane, "Arrival modeling and error analysis for molecular communication via diffusion with drift," in *Proceedings of the Second Annual Int. Conf. on Nanoscale Computing and Communication*, ser. NANOCOM' 15. New York, NY, USA: ACM, 2015, pp. 26:1–26:6.

- [73] H. V. Poor, *An Introduction to Signal Detection and Estimation (2Nd Ed.)*. New York, NY, USA: Springer-Verlag New York, Inc., 1994.
- [74] P. K. Varshney, C. S. Burrus, and C. Sidney, *Distributed detection and data fusion*, ser. Signal processing and data fusion. New York: Springer, 1997.
- [75] R. A. Johnson and D. W. Wichern, *Applied multivariate statistical analysis*. Upper Saddle River: Pearson Prentice hall, 2007, edition internationale.
- [76] P. K. Varshney, *Distributed Detection and Data Fusion*, 1st ed. Secaucus, NJ, USA: Springer-Verlag New York, Inc., 1996.